

Homodimeric Bis-Quaternary Heterocyclic Ammonium Salts as Potent Acetyl- and Butyrylcholinesterase Inhibitors: A Systematic Investigation of the Influence of Linker and Cationic Heads over Affinity and Selectivity

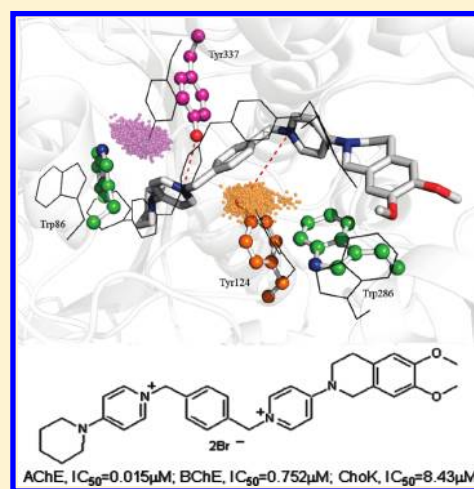
Ana Conejo-García,^{†,‡} Leonardo Pisani,^{†,‡} Maria del Carmen Núñez,[†] Marco Catto,[‡] Orazio Nicolotti,[‡] Francesco Leonetti,[‡] Joaquín M. Campos,[†] Miguel A. Gallo,[†] Antonio Espinosa,[†] and Angelo Carotti^{*,‡}

[†]Departamento de Química Farmacéutica y Orgánica, Facultad de Farmacia, Universidad de Granada, Campus de Cartuja, 18071 Granada, Spain

[‡]Dipartimento Farmacochimico, Università degli Studi di Bari "Aldo Moro", Via E. Orabona, 4, 70125 Bari, Italy

S Supporting Information

ABSTRACT: A molecular library of quaternary ammonium salts (QASs), mainly composed of symmetrical bis-quaternary heterocyclic bromides exhibiting choline kinase (ChoK) inhibitory activity, were evaluated for their ability to inhibit acetyl- and butyrylcholinesterase (AChE and BChE, respectively). The molecular framework of QASs consisted of two positively charged heteroaromatic (pyridinium or quinolinium) or sterically hindered aliphatic (quinuclidinium) nitrogen rings kept at an appropriate distance by lipophilic rigid or semirigid linkers. Many homodimeric QASs showed AChE and BChE inhibitory potency in the nanomolar range along with a low enzymatic selectivity. Computational studies on AChE, BChE, and ChoK allowed identification of the key molecular determinants for high affinity and selectivity over either one of the three enzymes and guided the design of a hybrid bis-QAS (**56**) exhibiting the highest AChE affinity ($IC_{50} = 15$ nM) and selectivity over BChE and ChoK ($SI = 50$ and 562 , respectively) and a promising pharmacological potential in myasthenia gravis and neuromuscular blockade.



INTRODUCTION

Acetylcholine (ACh) is a neurotransmitter in both the peripheral and central nervous system (PNS and CNS, respectively). In the PNS, ACh mediates nerve impulse in neuromuscular junctions and is a major neurotransmitter in the autonomic nervous system, whereas in the CNS, it chiefly controls memory and learning processes.

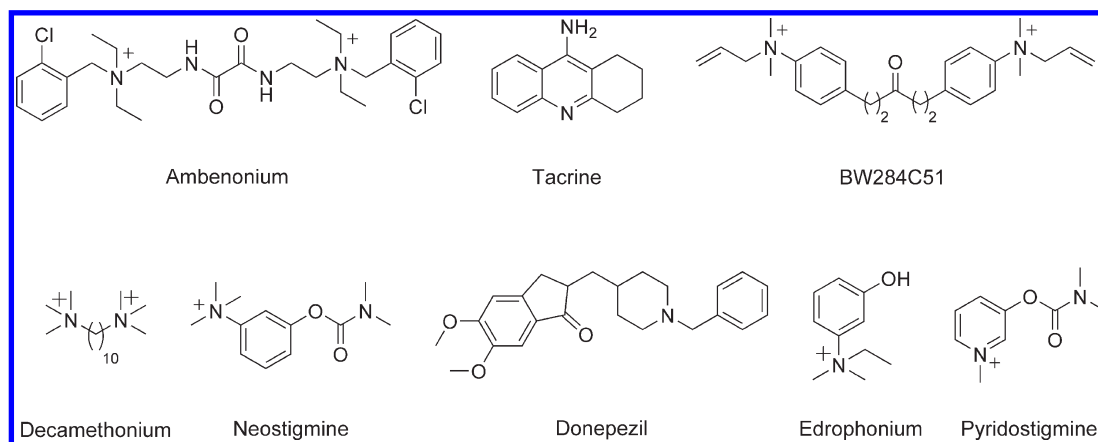
Two cholinesterases (ChEs), which are serine hydrolase enzymes, contribute to the degradation of the neurotransmitter ACh; they are acetylcholinesterase (AChE, EC 3.1.1.7) and butyrylcholinesterase (BChE, EC 3.1.1.8). Both ChEs hydrolyze ACh, albeit with slightly different kinetics, and coexist ubiquitously in humans. AChE, mainly expressed in the muscle and cholinergic nervous system, shows a selectivity toward its endogenous substrate higher than BChE, which is produced in the liver and represents the predominant plasmatic ChE. The two ChEs are encoded by different genes and differ in substrate specificity and sensitivity to inhibitors mainly because of significant structural differences in their active site gorge.^{1,2} AChE enzymatic cavity has the shape of a narrow gorge nearly 20 Å deep, lined with 14 highly conserved

aromatic residues at the bottom where the active site is located.³ Here, two different and close subsites contribute to acetylcholine binding (primary anionic subsite) and hydrolytic activity (esteratic subsite). One of the most significant structural differences between the two ChEs resides in their peripheral binding site. In the AChE, where it gives rise to more specific interactions with ligands, it is called the peripheral anionic subsite (PAS) and it is smaller and narrower than in BChE. In addition, consolidated experimental evidence supports the involvement of PAS in the acceleration of amyloid β peptide ($A\beta$) aggregation in the CNS leading to senile plaques that represent the major histopathological hallmarks of Alzheimer's disease (AD).⁴ A strong binding at the PAS accounts for the high inhibitory potency toward peripheral AChE of many gorge-spanning, highly polar bis-quaternary ammonium salts (QASs), e.g., decamethonium and ambenonium, whereas less polar gorge-spanning aminic compounds (e.g., donepezil and homo- and heterodimers of tacrine), targeting mainly the central AChE, bind

Received: October 8, 2010

Published: March 21, 2011

Chart 1. Chemical Structures of Different AChE Inhibitors Cited in the Text



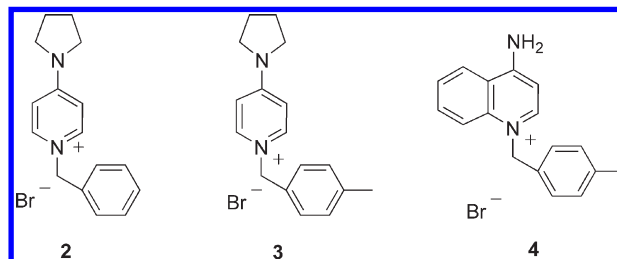
at the PAS with one of the two molecular heads as revealed by many cocrystallized enzyme–inhibitors complexes.⁵

The interest in AChE as a biological target in pharmaceutical research arises from the large number of potential central and peripheral therapeutic activities of AChE inhibitors. More recently developed AChE inhibitors (AChE-Is) address the symptomatic treatment of AD,⁶ while older QASs AChE-Is have found a therapeutic application in the treatment of neuromuscular blockade (NMB) in surgical anesthesia,⁷ myasthenia gravis (MG),⁸ and to a lesser extent in glaucoma. As for the NMB reversal agents, at present, all clinically used drugs, such as neostigmine, pyridostigmine, and edrophonium, are QASs inhibitors of AChE. While for glaucoma the currently used drugs are β -blockers and prostaglandin analogues,⁹ in the case of MG, a debilitating and rare autoimmune disease involving a progressive aberration of the neuronal transmission at the neuromuscular junctions, the first-line treatment in the early stage and in mild disease is still made with oral and low brain-permeable AChE-Is (e.g., the QASs pyridostigmine and neostigmine). To reduce the major drawbacks associated with this therapy resulting in the so-called cholinergic crisis (e.g., hypersalivation, muscular weakness, diarrhea, and cardiovascular side effects),¹⁰ the search for new more potent and selective peripheral AChE-Is is still ongoing.

Indeed, over the years a plethora of potent and selective AChE-Is have been reported, showing a wide range of chemical diversity and biopharmacological actions. Within this broad cluster of chemical entities, mono- and bis-QASs have kept a starring role. The bis-QASs are generally spanning along the deep gorge of AChE binding to both primary and peripheral anionic subsites which are characterized by the presence of Trp residues (e.g., Trp84 and Trp279, respectively, in *Torpedo californica* AChE (TcAChE)). Therefore, a number of bis-QASs proved to display outstanding nano- or subnanomolar affinities because of the highly positive binding stabilization by cation– π interactions with Trp residues in both AChE subsites and, more occasionally, by polar interactions within the spanning gorge. As an example, the excellent affinity of ambenonium (IC_{50} = 0.12 nM) and BW284C51 (IC_{50} = 8 nM), two symmetrical bis-QASs (Chart 1), might be ascribed to these multiple strong interactions.

The variety of pharmacological activities displayed by QASs, their generally facile synthetic accessibility, and our consolidated expertise in the study of the inhibition of AChE and BChE by

Chart 2. Chemical Structures of Mono-Quaternary Ammonium Salts 2–4



heterodimeric edrophonium–coumarin hybrids¹¹ prompted us to evaluate as ChEs inhibitors, with potential in MG and NMB, a large series of mono- (Chart 2), bis- (Chart 3), and tris-quaternary heterocyclic bromides (Chart 4). A number of these molecules had been already studied as ChoK inhibitors.^{12–20} The present research project stemmed from the observation that some key molecular features for an effective inhibition of ChEs were present in many ChoK inhibitors reported in Charts 2–4. In particular, the key pharmacophoric elements, which are two charged quaternary ammonium moieties kept at an appropriate distance by a linker, characterized many bis-QASs reported in Chart 3.

After an initial screening of AChE and BChE inhibition of already reported QASs,^{13–20} many new compounds were designed and tested aiming at the detection of the main molecular determinants of inhibitory potency and enzyme selectivity through an extension and a critical examination of the structure–affinity relationships (SAFIRs) and structure–selectivity relationships (SSRs).

Following one of the most exploited design strategy for enhancing AChE affinity, which is the dimerization of simple molecular fragments acting on the catalytic or peripheral binding sites, new and more selective inhibitors were designed by linking twin cationic heads with a spacer of appropriate length and flexibility with the purpose of discovering new molecules with high AChE affinity and potential pharmacological activity in glaucoma, myasthenia gravis, and neuromuscular blockade. Another important goal of our project was the dissociation of the ChE activity from the ChoK activity. Very satisfactorily, a

Chart 3. Chemical Structures of Bis-Quaternary Ammonium Salts 5–52

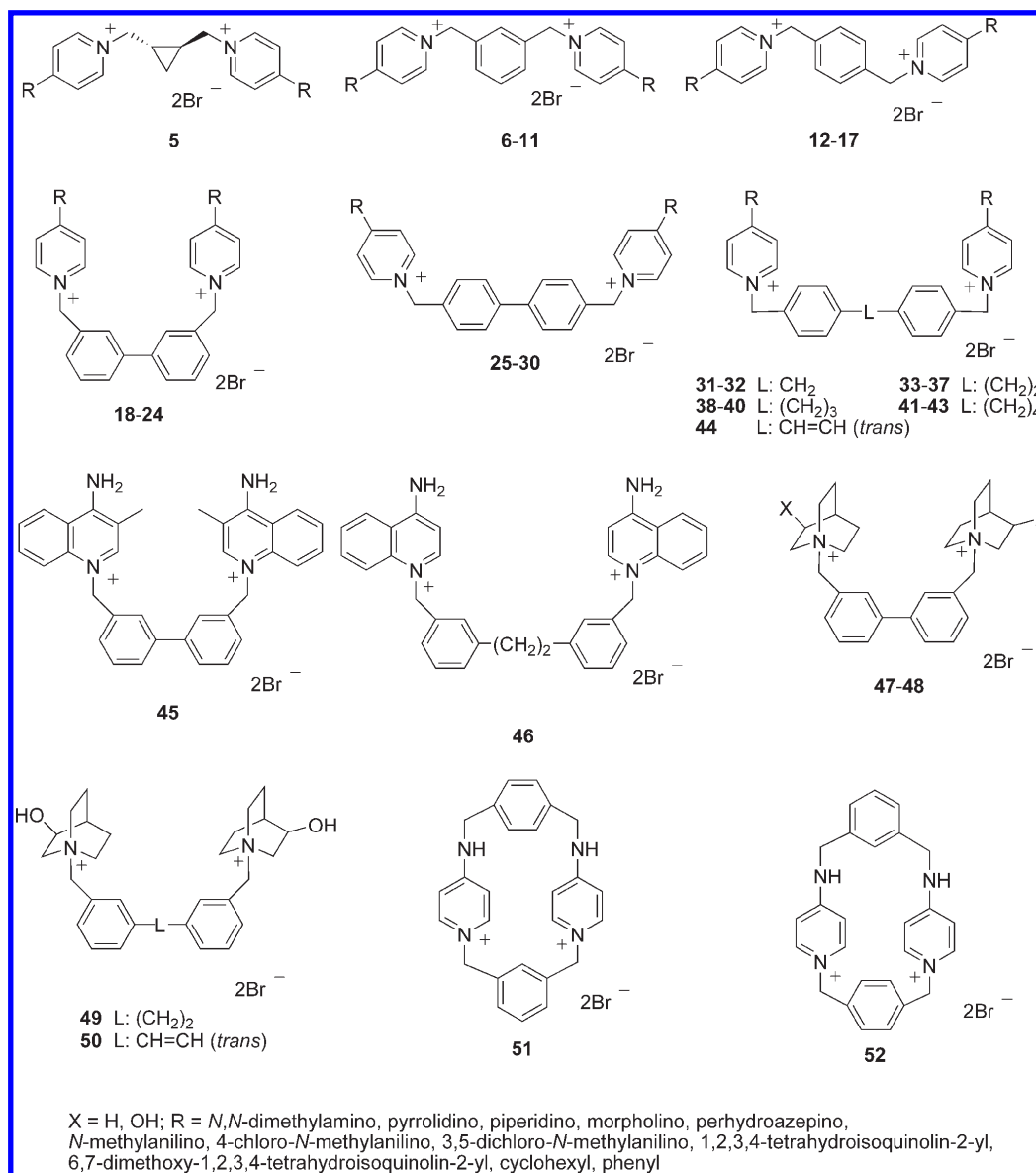
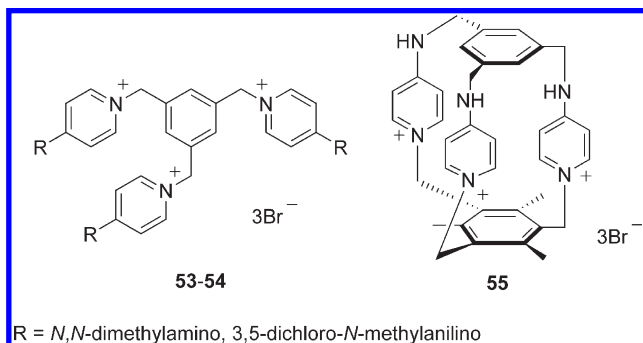


Chart 4. Chemical Structures of Tris-Quaternary Ammonium Salts 53–55



molecule with excellent inhibitory potency toward AChE, with good AChE over BChE selectivity, with outstanding AChE over

ChoK selectivity, and with a promising potential in MG and NMB was successfully designed, synthesized, and tested.

CHEMISTRY

The QASs presented in this paper are monocationic (Chart 2), bis-cationic (Chart 3), and tris-cationic derivatives (Chart 4). Thirty compounds have been prepared following procedures already described in the literature.^{13–20}

Concerning the synthesis of the new target QASs, the preparation of monocationic derivatives 2–4 was carried out by heating the appropriate nitrogen heterocycle with an equimolar ratio of benzyl or *p*-tolyl bromide in a sealed tube at 100 °C using 2-butanone as the solvent (Scheme 1).

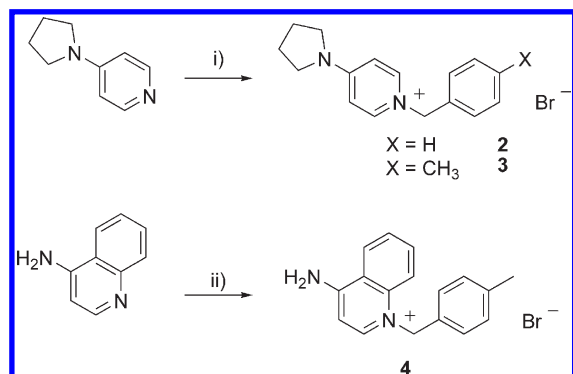
The synthesis of different dibromides was required to insert a linker between the two cationic fragments of new designed homodimeric QASs. *trans*-1,2-Bis(bromomethyl)cyclopropane was obtained by reduction of the corresponding commercial diester

to diol with lithium aluminum hydride²¹ and by the subsequent bromination with phosphorus tribromide.²² The 3,3'-bis(bromomethyl)biphenyl linker was prepared through the radical bromination of the commercially available 3,3'-dimethylbiphenyl with NBS and benzoyl peroxide as radical initiator.²³ The synthesis of 4,4'-bis(bromomethyl)biphenyl was carried out by reacting biphenyl with formaldehyde and hydrogen bromide in the presence of *o*-phosphoric acid.²⁴ 1,4-Bis[4-(bromomethyl)phenyl]butane was prepared by the catalytic hydrogenation of *trans,trans*-1,4-diphenyl-1,3-butadiene using Pd/C in glacial acetic acid, followed by the bis-bromomethylation in the previously mentioned conditions.²⁴ *trans*-4,4'-Bis(bromomethyl)stilbene was synthesized from *trans*-4,4'-bis(hydroxymethyl)stilbene by bromination with phosphorus tribromide.²⁵ *trans*-4,4'-Bis(hydroxymethyl)stilbene was prepared by the reduction of *trans*-dimethylstilbene 4,4'-dicarboxylate with lithium aluminum hydride.²⁶

Scheme 2 describes the preparation of 4,4'-bis(bromomethyl)biphenyl **1c** starting from the commercially available biphenyl-4,4'-dicarboxylic acid that was reacted with SOCl₂ to give the intermediate acyl chloride that afforded the ethyl diester **1a** upon refluxing in ethanol. LiAlH₄ in refluxing THF was used to reduce the diester **1a** to the corresponding diol **1b**. The subsequent bromination performed with CBr₄ and triphenylphosphine afforded dibromide **1c**.

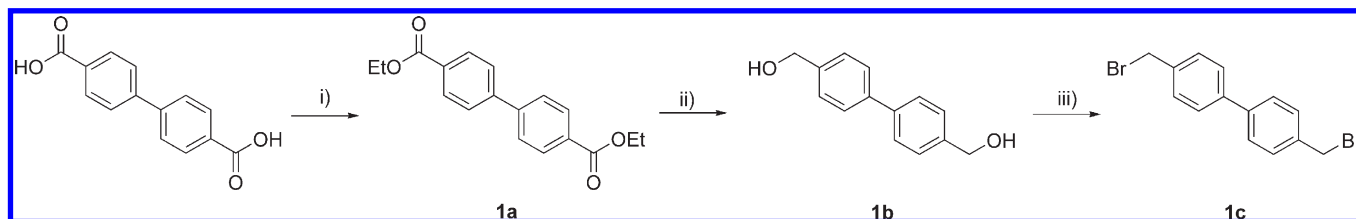
As shown in Scheme 3, a common synthetic pathway led to the targeted para-substituted pyridines **1d**, **1e**, and **1f** involving the microwave-assisted nucleophilic aromatic substitution of 4-chloropyridine with piperidine, 1,2,3,4-tetrahydroisoquinoline, and 6,7-dimethoxy-1,2,3,4-tetrahydroisoquinoline, respectively,

Scheme 1. Reaction Pathways for the Synthesis of Mono-QASs 2–4^a



^a Reagents and conditions: (i) benzyl or *p*-tolyl bromide, 2-butanone, sealed tube, 100 °C, 48 h; (ii) *p*-tolyl bromide, 2-butanone, sealed tube, 100 °C, 48 h.

Scheme 2. Synthesis of 4,4'-Bis(bromomethyl)biphenyl **1c^a**

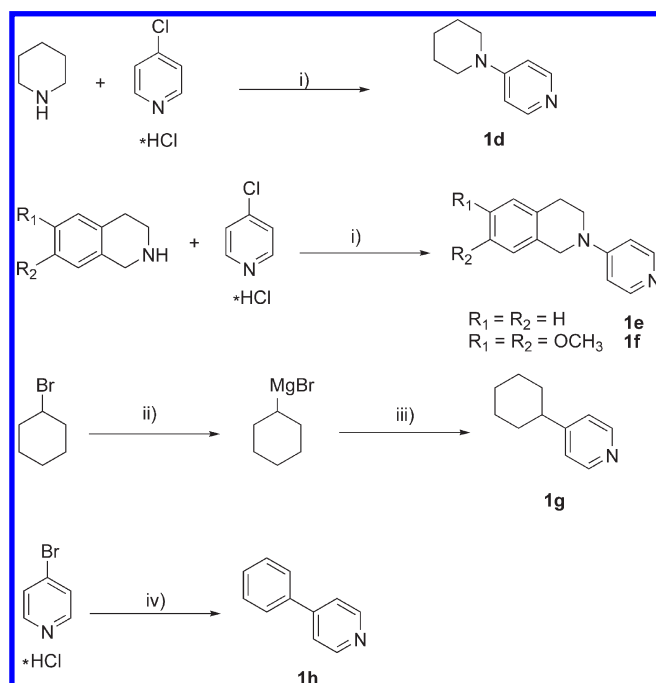


^a Reagents and conditions: (i) thionyl chloride, absolute ethanol, room temperature, overnight then reflux, 24 h; (ii) LiAlH₄, dry THF, reflux, 7 h; (iii) triphenylphosphine, CBr₄, dry CH₂Cl₂, 0 °C to room temperature, 6 h.

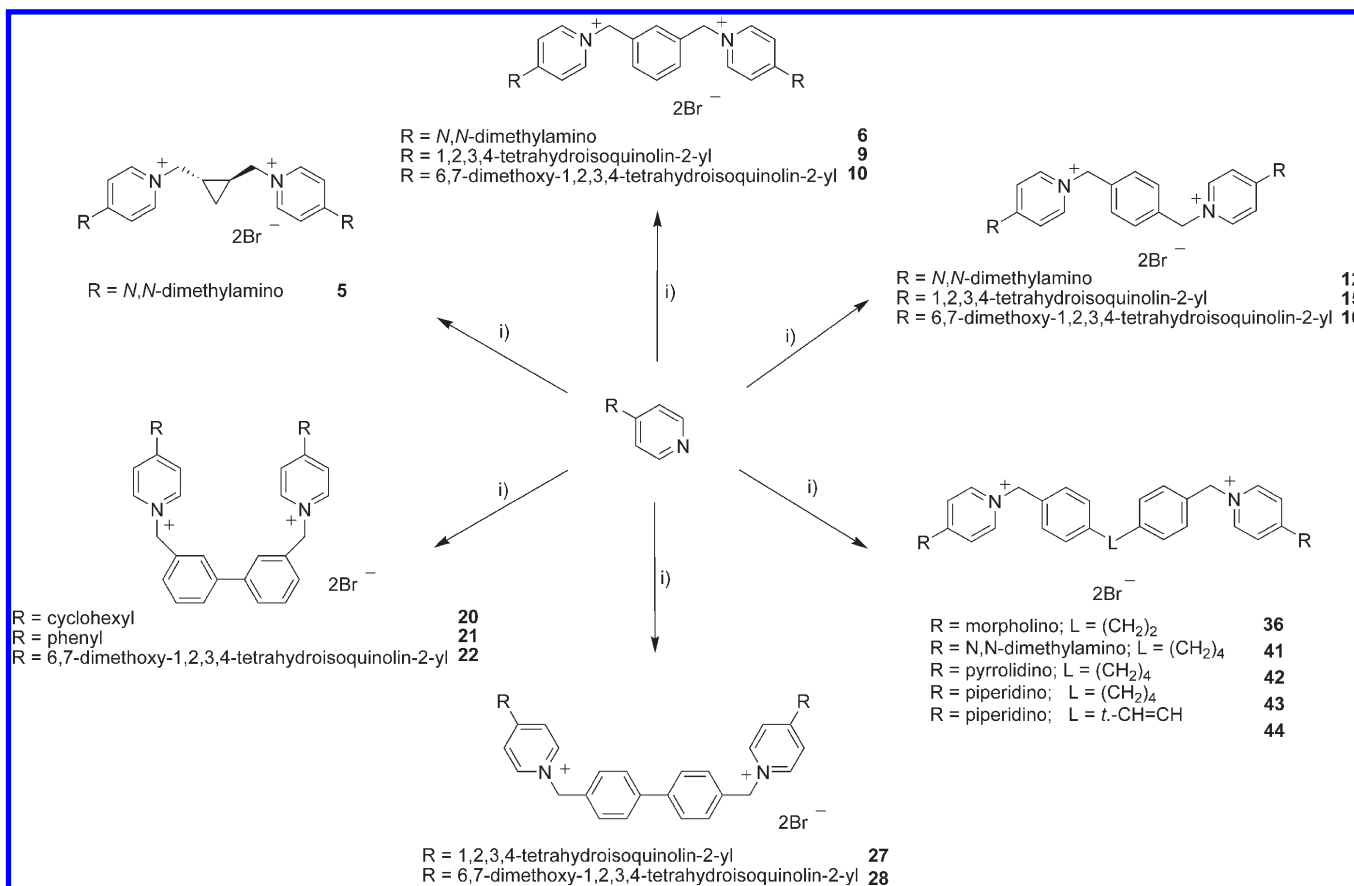
in acetonitrile at 160 °C. 4-Cyclohexylpyridine **1g** was prepared by an iron-mediated coupling reaction between 4-chloropyridine¹³ and freshly prepared cyclohexylmagnesium bromide, using THF as the solvent and NMP as the ligand. The Grignard reagent was prepared in situ by classic halogen–metal exchange reaction starting from cyclohexyl bromide and magnesium turnings in refluxing THF, in the presence of a catalytic amount of iodine (Scheme 3). A Suzuki coupling reaction between 4-chloropyridine hydrochloride and phenylboronic acid, in the presence of Pd-tetrakis(triphenylphosphine) as Pd(0) source and Cs₂CO₃ as the base in a dimethoxyethane/water solvents mixture, allowed the synthesis of 4-phenylpyridine **1h** as described in Scheme 3.

The synthesis of the new target homodimeric bis-QASs was carried out by heating the suitable dibromides and the appropriate nitrogen heterocycles (namely, 4-substituted pyridines or substituted quinolines and quinuclidines) in a molar ratio 1:2, thus obtaining the bis-cationic derivatives **5**, **6**, **9**, **10**, **12**, **15**, **16**, **20–22**, **27**, **28**, **36**, **41–44** (Scheme 4), and **47–50** (Scheme 5).

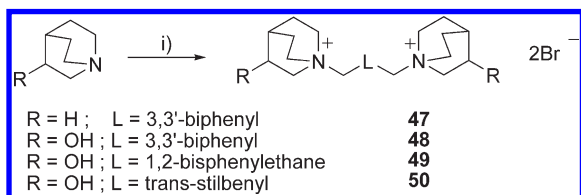
Scheme 3. Synthesis of 4-Substituted Pyridines **1d–h^a**



^a Reagents and conditions: (i) *N,N*-diisopropylethylamine, dry acetonitrile, 160 °C, microwave, 1 h; (ii) magnesium turnings, iodine, dry THF, reflux, 1 h; (iii) 4-chloropyridine, Fe(acac)₃, THF, NMP, room temperature, 15 h; (iv) phenylboronic acid, Cs₂CO₃, Pd-tetrakis(PPh₃), dimethoxyethane/water 4/1, 80 °C, 4 h.

Scheme 4. Reaction Pathway for the Synthesis of Symmetrical Bis-QASs 5, 6, 9, 10, 12, 15, 16, 20–22, 27, 28, 36, and 41–44^a

^a Reagents and conditions: (i) appropriate dibromides, 2-butanone, sealed tube, 100 °C, 15–192 h.

Scheme 5. Reaction Pathway for the Synthesis of Symmetrical Bis-QASs 47–50^a

^a Reagents and conditions: (i) appropriate dibromides, 2-butanone, sealed tube, 100 °C, 15–192 h.

The reactions were performed in a sealed tube at 100 °C using 2-butanone as the solvent.

Scheme 6 depicts the synthesis of the heterodimeric compound **56**. Intermediate monobromide **1i** was obtained through the nucleophilic substitution of 4-substituted pyridine **1d** with an excess of 1,4-bis(bromomethyl)benzene in 2-butanone in a sealed tube at 100 °C. Then **1i** was reacted in the same conditions with an equimolar ratio of tetrahydroisoquinoline derivative **1f**, yielding the desired heterodimer **56**.

BIOLOGICAL ASSAYS

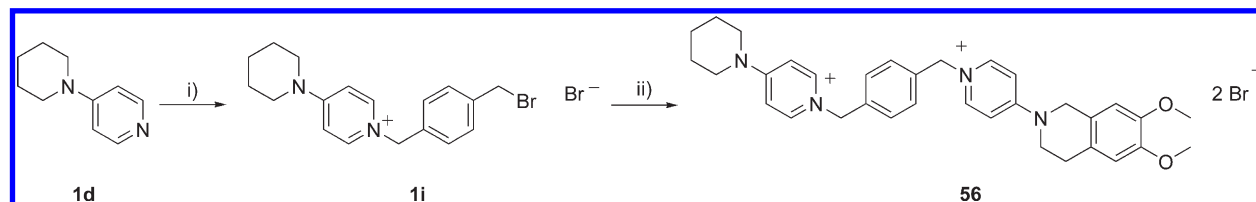
The ChEs *in vitro* inhibition data of the examined QASs, determined by using the Ellman's assay,²⁷ are reported in Tables 1–5. ChoK inhibitory activity of compound **56** was

assessed in an *ex vivo* system using recombinant human enzyme according to a reported method.¹³ Inhibition of β -amyloid aggregation (Table 5) was determined with a spectrofluorimetric, thioflavin-T based assay as previously described.²⁸

MOLECULAR MODELING

The program GOLD²⁹ was used in all the docking simulations. GOLD offers two standard fitness functions, which are GoldScore and ChemScore, with generally comparable performances. However, for any given problem, their predictive capability might strongly differ, and therefore, the selection of the fitness function is generally made after assessing its capacity to accurately reproduce the X-ray binding conformations. In our case, the two functions were challenged in the prediction of the binding conformations of donepezil and hemicholinium-3, found in their complexes with *TcAChE* (PDB code 1EVE)⁵ and *hChoK* (PDB code 3F2R),³⁰ respectively. As a measure of fit, the rmsd value was calculated over all the corresponding heavy atoms between the docking and crystal conformations. As GoldScore afforded better results for ChEs while ChemScore was better calibrated toward ChoK, the two different fitness functions were accordingly selected for the docking runs on ChEs and ChoK, respectively. The rmsd values for donepezil and hemicholinium-3 were as small as 0.99 and 1.53 Å, respectively.

Molecular dynamics (MD) simulations were carried out by using a periodic box of TIP3P water molecules extended for 18 Å from the protein atoms which were modeled with the parm03

Scheme 6. Synthesis of Heterodimer Bis-QAS 56^a

^a Reagents and conditions: (i) 1,4-bis(bromomethyl)benzene (excess), 2-butanone, 100 °C, sealed tube, 120 h; (ii) **1f**, 2-butanone/acetonitrile 4/1, 100 °C, sealed tube, 48 h.

Table 1. Biological Data of Monomeric Pyridinium Compounds 2–4

| Compd | Structure ^a | AChE ^b | BChE ^b |
|-------|------------------------|-------------------|-------------------|
| 2 | | 5.53 | 28.1±2% |
| 3 | | 52.0±3% | 20.4±2% |
| 4 | | 34.0±2% | 53.2±3% |

^a Counterions are always bromide ions. ^b The AChE and BChE inhibitory activities are expressed as IC₅₀ (μM) or as percentage of inhibition ± SEM at 10 μM. Values are the mean of two or three independent experiments. SEM of IC₅₀ values are <10%.

force field. Energy minimization was executed by using AMBER, version 10,³¹ while a 5 ns MD simulation was performed with NAMD.³²

RESULTS AND DISCUSSION

The influence of the cationic heads and linkers on the AChE and BChE inhibitory activity was extensively explored with appropriate structural modifications that allowed us to shed light on the most salient aspects of the SAFIRs and SSRs.

Inhibition data are reported in Tables 1–5 as IC₅₀ (μM) or as percentage of inhibition at 10 μM. The enzyme selectivity was expressed with the selectivity index SI, which is the IC₅₀(BChE)/IC₅₀(AChE) affinity ratio.

Inhibitors were grouped according to their shared linkers in the following order: monocationic (Table 1), bis-cationic (Tables 2–4), and tris-cationic (Table 4) QASs. For the sake of clarity, after some general comments on the SAFIRs and SSRs, SAFIRs will be discussed separately for AChE and BChE inhibition.

General Observations on SAFIRs and SSRs. For an immediate and more efficient analysis of SAFIRs and SSRs, inhibition data are presented in Figure 1 as a plot of pIC₅₀ of AChE (*x*-axis) versus pIC₅₀ of BChE (*y*-axis) using the same scale and range for both axes (square plot). To avoid the loss of informative data points, compounds **12**, **48**, and **53**, for which only the percentage of inhibition of one ChE was available, were added to the plot with an estimated missing pIC₅₀ of 5.00. Compounds with close affinities at both ChEs lie on the bisector (*y* = *x*) of the graph, whereas selective AChE and BChE inhibitors lie below and above

the bisector, respectively, the distance of their pIC₅₀ values from the bisector being a direct measure of their degree of selectivity. Two parallel lines traced at one pIC₅₀ unit distance below and above the bisector enable the straightforward location of inhibitors with a SI higher than 10 and lower than 0.1, respectively (that is, ΔpIC₅₀ > 1 and ΔpIC₅₀ < −1, respectively).

At first glance, the plotted data indicated that a large number of potent AChE inhibitors were discovered (i.e., compounds **8**, **14**, **15**, **18**, **19**, **20**, **25**, **28**, **32**, **35**, **37**, **38**, **42**, **43**, and **49** with an IC₅₀ mean value close to 90 nM) whereas only few BChE inhibitors (i.e., compounds **32**, **35**, **45**, and **47**) exhibited a comparable high potency. The same considerations hold for the enzymatic selectivity: a relatively high number of inhibitors showed good AChE selectivity (SI > 10), whereas only compound **47** exhibited a good BChE selectivity (SI < 0.1).

Monocationic compounds 2–4 and bis-quaternary pyridinium derivative **5**, bearing a cyclopropyl linker, showed low binding affinities for both ChEs.

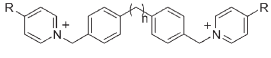
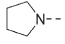
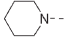
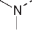
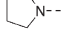
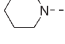
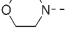
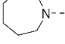
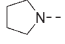
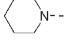
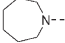
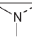
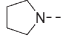
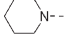
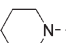
SAFIRs of AChE Inhibition. Among derivatives 5–44, characterized by a common bis-pyridinium cationic head carrying various, generally basic, R-substituents at position 4, very interesting IC₅₀ values (≤ 100 nM) were observed for compounds **14**, **18**, **19**, **25**, **28**, **32**, **35**, **37**, **38**, and **43**. A high AChE binding affinity seemed to be related to the presence of differently substituted lipophilic aromatic rings in the linker that might interact with aromatic amino acid side chains spanning the aromatic gorge of the enzymatic cavity. Actually, moving from a cyclopropyl to a more lipophilic phenyl linker, a significant increase of affinity can be appreciated (compare **5**, IC₅₀ = 8.78 μM, with **6** and **12**, IC₅₀ = 0.390 and 1.31 μM, respectively).

Regarding compounds bearing xylyl spacers, an increasing size of the 4-substituent in the cationic heads from *N,N*-dimethylamino to the piperidinyl group resulted in a significant gain of activity in both *p*- and *m*-xylyl linkers (**14** > **13** > **12** and **8** > **7** > **6**). When the aliphatic amino substituents were substituted with larger and more lipophilic 1,2,3,4-tetrahydroisoquinolin-2-yl (THIQ) moieties, a drop of affinity was observed (**8** > **9** > **10** and **14** > **15** > **16**), the worst results being obtained with the 6,7-dimethoxy-THIQ derivatives **10** and **16** (IC₅₀ = 2.10 and 1.95 μM, respectively). Interestingly, this decrease of affinity was less dramatic in the series of inhibitors with a *p*-xylyl linker. It may be that more sterically hindered cationic heads were better tolerated when tethered by a *p*-xylyl than a *m*-xylyl spacer because the former might allow a more extended and stable binding conformation. This hypothesis may hold also for sterically hindered cationic heads tethered to the longer 3,3'-bis-methylene- and 4,4'-bis-methylenebiphenyl isomeric linkers (compare **28** with **22**). Moreover, compounds bearing 3,3'-bis-methylenebiphenyl spacers were more active than the corresponding meta-substituted xylyl-linked analogues (**18** > **7**, **19** > **8**, and **22** > **10**). Within

Table 2. Biological Data of Dimeric Pyridinium Compounds 5–44

| General Structure ^a | Compd | R ^b | AChE ^c | BChE ^c | SI ^d |
|--------------------------------|-------|----------------|-------------------|-------------------|-----------------|
| | 5 | | 8.78 | 12.4±1% | n.d. |
| | 6 | | 0.390 | 7.56 | 19 |
| | 7 | | 0.162 | 2.20 | 14 |
| | 8 | | 0.114 | 0.335 | 2.9 |
| | 9 | | 0.281 | 0.190 | 0.68 |
| | 10 | | 2.10 | 0.890 | 0.42 |
| | 11 | | 1.15 | 0.910 | 0.79 |
| | 12 | | 1.31 | 50.3±1% | 7.6 |
| | 13 | | 0.336 | 1.30 | 3.9 |
| | 14 | | 0.072 | 0.682 | 9.5 |
| | 15 | | 0.126 | 0.327 | 2.6 |
| 16 | | 1.95 | 1.37 | 0.70 | |
| 17 | | 5.20 | 1.60 | 0.31 | |
| | 18 | | 0.039 | 0.518 | 13 |
| | 19 | | 0.026 | 0.179 | 6.9 |
| | 20 | | 0.134 | 1.09 | 8.2 |
| | 21 | | 0.553 | 0.797 | 1.4 |
| | 22 | | 0.519 | 1.17 | 2.3 |
| | 23 | | 0.869 | 0.399 | 0.46 |
| | 24 | | 1.78 | 0.496 | 0.28 |
| | 25 | | 0.090 | 1.27 | 14 |
| 26 | | 0.160 | 0.430 | 2.7 | |
| 27 | | 0.346 | 0.318 | 0.92 | |
| 28 | | 0.094 | 1.53 | 16 | |
| 29 | | 3.07 | 0.683 | 0.22 | |
| 30 | | 2.87 | 0.550 | 0.19 | |

Table 2. Continued

| General Structure ^a | Compd | R ^b | AChE ^c | BChE ^c | SI ^d | |
|---|-------|----------------|---|-------------------|-----------------|------|
|  | 31 | n = 1 |  | 0.183 | 0.576 | 3.1 |
| | 32 | |  | 0.083 | 0.062 | 0.75 |
| | 33 | |  | 0.628 | 1.36 | 2.2 |
| | 34 | |  | 0.385 | 0.735 | 1.9 |
| | 35 | n = 2 |  | 0.079 | 0.130 | 1.6 |
| | 36 | |  | 2.67 | 4.48 | 1.7 |
| | 37 | |  | 0.086 | 0.274 | 3.2 |
| | 38 | |  | 0.081 | 0.292 | 3.6 |
| | 39 | n = 3 |  | 0.163 | 0.149 | 0.91 |
| | 40 | |  | 0.202 | 0.163 | 0.81 |
| | 41 | |  | 0.252 | 0.372 | 1.5 |
| | 42 | n = 4 |  | 0.104 | 0.671 | 6.5 |
| | 43 | |  | 0.100 | 0.206 | 2.1 |
| | 44 | |  | 0.582 | 0.247 | 0.42 |

^a Counterions are always bromide ions. ^b Dashed lines represent the connection bond of the substituent. ^c The AChE and BChE inhibitory activities are expressed as IC₅₀ (μ M) or as percentage of inhibition \pm SEM at 10 μ M. Values are the mean of two or three independent experiments. SEM of IC₅₀ values are <10%. ^d SI is the selectivity index, that is, the IC₅₀(BChE)/IC₅₀(AChE) affinity ratio.

this class of compounds the most potent AChE inhibitor **19**, showing an IC₅₀ = 26 nM, was found.

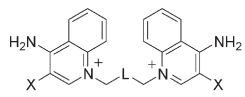
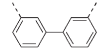
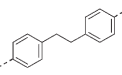
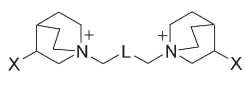
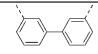
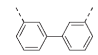
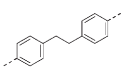
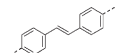
An increased flexibility of the spacer was obtained by introducing methylene bridges between the two phenyl rings of the 4,4'-bis-methylenephényl group (compounds **31**–**43** in Table 2). No clear SAFIRs emerged from the analysis of inhibition data of this series of more flexible inhibitors, and no optimal length of the linker could be found. However, in the presence of more flexible linkers very potent AChE inhibitors, i.e., compounds **32**, **35**, **37**, **38**, and **43**, all exhibiting IC₅₀ \leq 100 nM, emerged. In addition, it is worth noting that the reduction of flexibility in the linker and of the lipophilicity of the R group led to a significant decrease of AChE affinity (compare **44** vs **35** and **35** vs **36**, respectively).

The AChE enzymatic region likely binding the R substituents of the cationic heads appeared not so sterically hindered, as the five-, six- and seven-membered cycloaliphatic amines seemed to be bound with good binding affinities (see compounds **34**, **35**, and **37** and compounds **38**–**40**).

The presence of substituted or unsubstituted *N*-methylanilino R groups in the cationic heads of compounds **11**, **17**, **23**, **24**, **29**, and **30** promoted BChE selectivity. This result may be attributed to an increased lipophilic character and/or to some

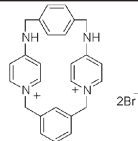
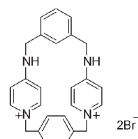
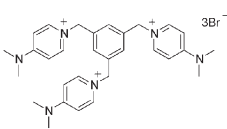
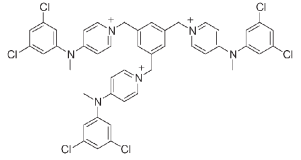
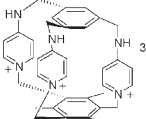
steric hindrance at the AChE binding site(s) not seen in the larger, and more accommodating, BChE binding cavity. An alternative explanation could be found in a different charge distribution likely resulting from the reduced electron-donor character of the anilino group compared to the cycloaliphatic amino groups. Actually, a strong electron-donor effect by R-substituents at position 4, and the consequent higher delocalization of the pyridinium positive charge, seemed to play a key role for good AChE affinity most likely because π -cation interactions with the aromatic residues in the PAS of AChE might be reinforced. And in fact, piperidine derivative **19** exhibited an affinity significantly higher than that of the comparably sized cyclohexyl (**20**) and phenyl (**21**) derivatives (IC₅₀ = 26 vs 134 and 553 nM, respectively), both having a lower electron-donating character. These findings were supported by semiempirical AM1 level calculations of the charge distribution and the LUMO (lowest unoccupied molecular orbital) energy of 1-methylpyridinium and of a series of 4-substituted derivatives, which are the 1-methyl-4-phenylpyridinium, 4-cyclohexyl-1-methylpyridinium, and 4-piperidinyl-1-methylpyridinium, used as reference model systems. The obtained results (data not shown) were in good agreement with

Table 3. Biological Data of Dimeric Quinolinium and Quinuclidinium Derivatives 45–50

| General Structure ^a | Compd | X | L ^b | AChE ^c | BChE ^c | SI ^d |
|---|-------|-----------------|---|-------------------|-------------------|-----------------|
|  | 45 | CH ₃ |  | 0.497 | 0.059 | 0.12 |
| | 46 | H |  | 0.672 | 0.620 | 0.92 |
|  | 47 | H |  | 1.10 | 0.089 | 0.081 |
| | 48 | OH |  | 55.8±6% | 1.15 | 0.11 |
| | 49 | OH |  | 0.097 | 2.09 | 22 |
| | 50 | OH |  | 0.141 | 5.34 | 38 |

^a Counterions are always bromide ions. ^b Dashed lines represent the connection bond of the substituent. ^c The AChE and BChE inhibitory activities are expressed as IC₅₀ (μM) or as percentage of inhibition ± SEM at 10 μM. Values are the mean of two or three independent experiments; SEM of IC₅₀ values are <10%. ^d SI is the selectivity index, that is, the IC₅₀(BChE)/IC₅₀(AChE) affinity ratio.

Table 4. Biological Data of Bis- and Tris-QASs 51–55

| Compd | Structure ^a | AChE ^b | BChE ^b | SI ^c |
|-------|---|-------------------|-------------------|-----------------|
| 51 |  | 3.90 | 0.850 | 0.22 |
| 52 |  | 4.80 | 2.30 | 0.48 |
| 53 |  | 2.75 | 52.6±2.1% | 3.6 |
| 54 |  | 1.77 | 0.679 | 0.38 |
| 55 |  | 3.68 | 0.516 | 0.14 |

^a Counterions are always bromide ions. ^b The AChE and BChE inhibitory activities are expressed as IC₅₀ (μM) or as percentage of inhibition ± SEM at 10 μM. Values are the mean of two or three independent experiments. SEM of IC₅₀ values are <10%. ^c SI is the selectivity index, that is, the IC₅₀(BChE)/IC₅₀(AChE) affinity ratio.

those reported in a previous investigation and unequivocally indicated that electron releasing effects, in particular by the

1-piperidiny substituent, increased charge delocalization and the LUMO character which were correlated with the potency of

Table 5. Human Cholinesterases and $A\beta$ Aggregation Inhibition Data

| compd | <i>h</i> AChE ^a | <i>h</i> BChE ^a | $A\beta_{1-40}$ ^b |
|-----------|----------------------------|----------------------------|------------------------------|
| 14 | 75 ± 13 | 610 ± 25 | not active |
| 19 | 60 ± 4 | 330 ± 14 | 30 ± 2 |
| 47 | 620 ± 45 | 36 ± 3 | not active |
| 56 | 62 ± 4 | 620 ± 55 | 15 ± 1 |
| donepezil | 18 ± 4 | 3900 ± 360 | not active |
| tacrine | 110 ± 5 | 23 ± 5 | not active |

^aThe *h*AChE (human recombinant) and *h*BChE (from human serum) inhibitory activities are expressed as IC₅₀ (nM). ^bPercentage of $A\beta$ (30 μ M) self-aggregation inhibition measured at 100 μ M test compound. Values are the mean ± SEM of at least three independent experiments.

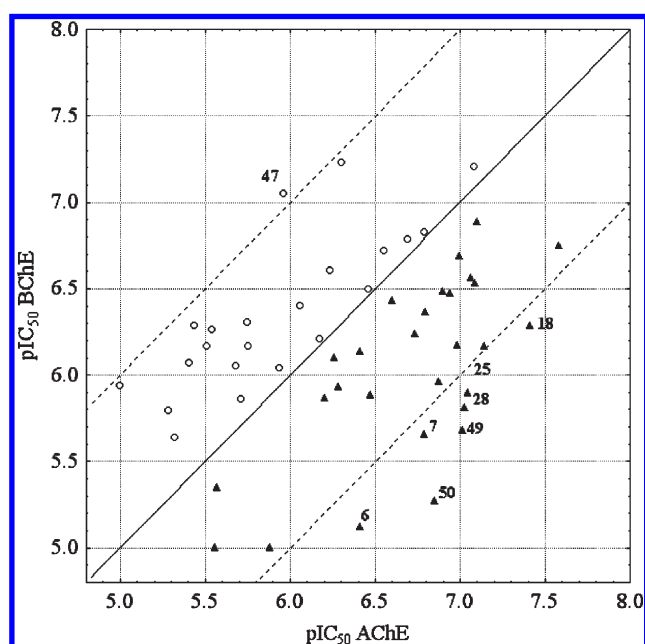


Figure 1. Square plot of AChE/BChE affinity and selectivity. Bordered by dashed lines, the bottom-right and upper-left corners contain potent and selective AChE (solid triangles) and BChE (empty circles) inhibitors, respectively. The solid line represents the bisector.

inhibition toward both AChE and BChE as a result of a weaker solvation effect.¹³

Compounds **45** and **46**, carrying the more lipophilic and bulkier 4-aminoquinolinium cationic heads, showed very low AChE affinity with both the 3,3'-bis-methylenbiphenyl (**45**) and the 1,2-bis-*p*-tolylethane (**46**) linker.

Also, derivative **47**, bearing very lipophilic and bulky quinuclidine cationic heads bound through a 3,3'-bis-methylenbiphenyl linker, exhibited a very low AChE affinity (IC₅₀ = 1.10 μ M) that was even worse when a hydroxyl group was introduced at position 3 in the quinuclidinium ring (compound **48**, 55.8% inhibition at 10 μ M). Conversely, bis-quinuclidine QASs **49** and **50** bearing a 1,2-bisphenylethane and a *trans*-stilbenyl linker, respectively, proved to be potent AChE inhibitors (IC₅₀ = 97 and 141 nM, respectively). Therefore, for the series of bis-quinuclidinium derivatives, both the flexibility and the length of the linker appeared to play a key role for an efficient interaction at the AChE binding sites.

Molecular rigidification represents a common strategy adopted by medicinal chemists to increase the activity of a drug or to reduce its side effects. Incorporating key functional groups of a flexible ligand into a ring is the usual way of “locking” a conformation and may provide valuable information on the likely active binding conformation of that ligand. With this aim, bispyridinium cyclophanes **51** and **52** had been prepared as ChoK inhibitors and were now tested as ChE inhibitors. All these very rigid macrocyclic compounds proved to be very poor AChE inhibitors (Table 4). The same poor inhibition data were obtained with the tris-cationic compounds **53–55**.

SAFIRs of BChE Inhibition. SAFIRs at BChE were not so sharply defined and clear as for AChE. Therefore, only a limited number, though important, of observations could be made.

BChE inhibition data in Tables 1–4 and in Figure 1 indicated that only compounds **32**, **45**, and **47**, exhibited IC₅₀ ≤ 100 nM. Two of them, compounds **45** and **47**, were characterized by bulky cationic heads, a structural feature previously hypothesized as responsible for the shift of selectivity toward BChE.

The large sized inhibitors listed in Table 4, with only one exception that is **53**, displayed a poor BChE affinity but higher than AChE.

Inhibitors with cationic heads carrying substituted or unsubstituted *N*-methylanilino R-groups showed a higher BChE inhibitory potency than AChE (see compounds **11**, **17**, **23**, **24**, **29**, and **30**). Notably, piperidiny-substituted inhibitors were always more potent than the corresponding pyrrolidiny derivatives, i.e., **8** > **7**, **14** > **13**, **19** > **18**, **26** > **25**, **32** > **31**, **35** > **34**, **39** > **38**, and **43** > **42**.

As far as the effect of linker flexibility on the BChE activity is concerned, it may be emphasized that a large number of potent BChE inhibitors, such as **32**, **35**, **39**, **40**, and **43** with IC₅₀ of 62, 130, 149, 163, and 206 nM, respectively, carried flexible linkers. However, this structural feature also determined a potent AChE inhibition, and as a result, inhibitors with high affinity toward both enzymes, e.g., compounds **32**, **35**, **39**, and **43**, might be found within this class of molecules.

SSRs. In general, no well-defined SSRs emerged from the analysis of the SI values, as the data variation was very limited. Moreover, the selectivity index SI comes from the ratio of two different experimental values (AChE and BChE IC₅₀ values), and therefore, it may suffer of a stronger error propagation compared to the single set of AChE and BChE affinity data. Consequently, only the most relevant aspects of the SSRs will be discussed.

AChE and BChE inhibition data in Tables 1–4 and in the plot of Figure 1 indicated that only a limited number of inhibitors showed a good selectivity toward AChE or BChE (SI > 10 or SI < 0.1, respectively). SI > 10 was exhibited by compounds **6**, **7**, **18**, **25**, **28**, **49**, and **50**, whereas only one compound (that is, **47**) displayed SI < 0.1. These compounds are highlighted in Figure 1 and are located below and above the parallel line traced at 1 log unit from the bisector, respectively.

The influence of the steric hindrance of the cationic heads and of the linker length and flexibility on the selectivity was not clearly defined. In general, a higher steric hindrance on both the cationic heterocycles and R-substituents increased the BChE affinity, but the resulting selectivity was generally not very high (see chloro-substituted *N*-methylanilino derivatives **17**, **24**, **29**, and **30**, the aminoquinolinium derivatives **45** and **46**, and all the large sized and/or rigid compounds **51**, **52**, **54**, and **55**). On the other hand, for the rigid and bulky quinuclidinium derivatives **47–50**, the length and, to a lesser extent, the flexibility of the

linker clearly appeared as crucial structural determinants for BChE or AChE selectivity. Compounds **49** and **50**, bearing a 1,2-*bis-p*-tolyl ethane and a 4,4'-*bis*-methylene-*trans*-stilbenyl linker, respectively, proved to be highly potent ($IC_{50} = 97$ and 141 nM, respectively) and selective AChE inhibitors ($SI = 22$ and 38 , respectively), whereas compound **48** with a shorter and less flexible 3,3'-methylenebiphenyl linker presented an inverted biological profile. In addition to this, derivative **47**, characterized by an unsubstituted quinuclidinium fragment, exhibited a high BChE affinity ($IC_{50} = 89$ nM) and the highest BChE selectivity within the whole series of tested molecules ($SI = 0.081$).

Finally a few words may be spent on the AChE over ChoK selectivity of the examined QASs. As previously noticed, some of the QASs reported in this work have been previously studied as ChoK inhibitors. The inhibition data on this enzyme varied from submicromolar to the high micromolar range, the very rigid cyclic bis-QAS **52** being the most potent ChoK inhibitor with an IC_{50} of $0.30 \mu M$ ¹⁸ and a low selectivity over AChE ($SI = 0.063$, where SI is the $IC_{50}(\text{ChoK})/IC_{50}(\text{AChE})$ affinity ratio). With the only exception of compound **23** ($IC_{50} = 0.40 \mu M$ ¹⁴ and $SI = 0.46$) all the other compounds (data not shown) exhibited $SI \gg 1$, with the highest selectivity displayed by compound **7** ($SI = 520$). AChE affinity of **7** was, however, relatively low ($IC_{50} = 162$ nM).

Structure-Based Design of an Inhibitor with Improved AChE Potency, AChE over BChE Selectivity, and AChE over ChoK Selectivity. Although a consistent number of homodimeric QASs exhibited AChE or BChE affinity in the nanomolar range, none of them showed a high selectivity toward either one of the two ChEs. A molecular hybridization approach was therefore conceived for the design of a potent and selective AChE inhibitor, possibly endowed with a low affinity toward the ChoK. This heterodimeric inhibitor was designed by exploring the combination of two differently 4-substituted pyridinium cationic heads, chosen among the ones characterizing the most active AChE inhibitors. Keeping in mind that the presence of an electron-releasing R-substituent at position 4 is crucial for good ChE affinity and that highly lipophilic and bulky R-substituents shifted the affinity toward BChE, unhindered electron-donating groups at position 4 (i.e., 1-pyrrolidinyl, 1-piperidinyl, and 1-azepinyl) were chosen as the substituent of one of the two pyridinium heads. Taking into account a previous observation that a low BChE affinity could have been promoted by the presence of only one hindered cationic head, the 6,7-dimethoxy-substituted and unsubstituted THIQ pyridinium moieties were explored as the second cationic head. Indeed the 6,7-dimethoxy-THIQ pyridinium cationic head proved to characterize very active AChE inhibitor (see compound **28**), providing that its potential steric hindrance was partly relieved by an elongated binding conformation, possibly ensured by para-disubstituted linkers. As far as ChoK inhibition is concerned, previous SAFIRs seemed to indicate that this choice could be compatible with a likely low inhibition. Accordingly, *p*-xylyl and the 4,4'-*bis*-methylenebiphenyl fragments were explored as the linkers of the two different cationic heads, selected on the basis of the previously discussed criteria. The study of the preferred binding conformations of potentially selective enzyme inhibitors derived from the combination of the just mentioned molecular fragments was carried throughout docking simulations.

For this study, the 3D coordinates of the human isoforms of AChE (PDB code 1B41), BChE (PDB code 1P0I), and ChoK (PDB code 3F2R) were retrieved from the Protein Data Bank. *hAChE* was chosen instead of *TcAChE* because it has almost

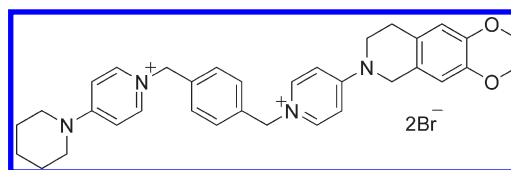


Figure 2. Heterodimer bis-QAS **56**.

identical amino acid residues at both the catalytic and peripheral binding sites, apart from the substitution of Tyr337 (*hAChE*) with Phe330 (*TcAChE*).³³ This single-residue change was not observed when analyzing primary sequences of either human (1B41, PDB entry) or bovine (AA123899.1, NCBI entry) AChEs.

A series of prospective docking studies were then undertaken to assist the rational design of a QAS inhibitor conceived to bind the three enzymes AChE, BChE, and ChoK, with highly different affinities. The task of identifying a novel potent AChE inhibitor with a remarkable selectivity over BChE and ChoK was very challenging because of the close sequence similarity between AChE and BChE (about 66%) and the greater structural diversity between the two ChEs and ChoK. In view of this, a large series of virtual compounds deriving from an exhaustive combination of the molecular features delineated above, i.e., two different cationic heads bound through para-substituted linkers, were employed to forecast, via molecular docking, AChE, BChE, and ChoK inhibition. Compounds exhibiting toward the three enzymes highly diverse affinities, as assessed by the different scoring energies, and binding modes compatible with those of known inhibitors (e.g., donepezil and decamethonium in the case of ChEs, and hemicholinium-3 in the case of ChoK) were selected and further analyzed for the evaluation of their synthetic feasibility. Among the investigated heterodimeric molecules, compound **56** was selected and synthesized as the most promising candidate (Figure 2).

It was in fact observed that the novel designed heterodimer **56** achieved a percentage of scoring vs donepezil equal to 102.9% for AChE and 103.5% for BChE, whereas vs hemicholinium-3 it was equal to 113.3% for ChoK. In addition, the visual inspection of its predicted posing into AChE, BChE, and ChoK (the last two reported in Figures S1 and S2, respectively, in the Supporting Information) disclosed to some extent a good overlap with binding modes of donepezil in *TcAChE* and hemicholinium-3 in *hChoK*. The most relevant difference between the docking pose of donepezil into *hAChE* (PDB code 1B41) and its experimental binding conformation into *TcAChE* (PDB code 1EVE) was the position of the piperidine ring which resulted more bent in *hAChE* and more distant from Tyr337 to prevent steric clashes. Such evidence was congruent with the observation that the overlay between the Tyr337 (*hAChE* numbering) and its equivalent Phe330 (*TcAChE* numbering) disclosed an rmsd equal to 1.99 \AA because of the structural fit induced by different cognate ligands within the two orthologous binding sites. However, a very nice match of the face-to-face interactions occurring at the catalytic and peripheral binding sites was observed.

As far as the docking of heterodimer **56** is concerned, it was observed that **56** was likely engaged in favorable interactions taking place simultaneously at both the primary and peripheral binding sites of *hAChE* with the top-scored docking pose exhibiting a GoldScore fitness energy equal to -51.69 kJ/mol . As shown in Figure 3, the prospective use of docking experiments suggested that the piperidinyl substituent was likely involved in

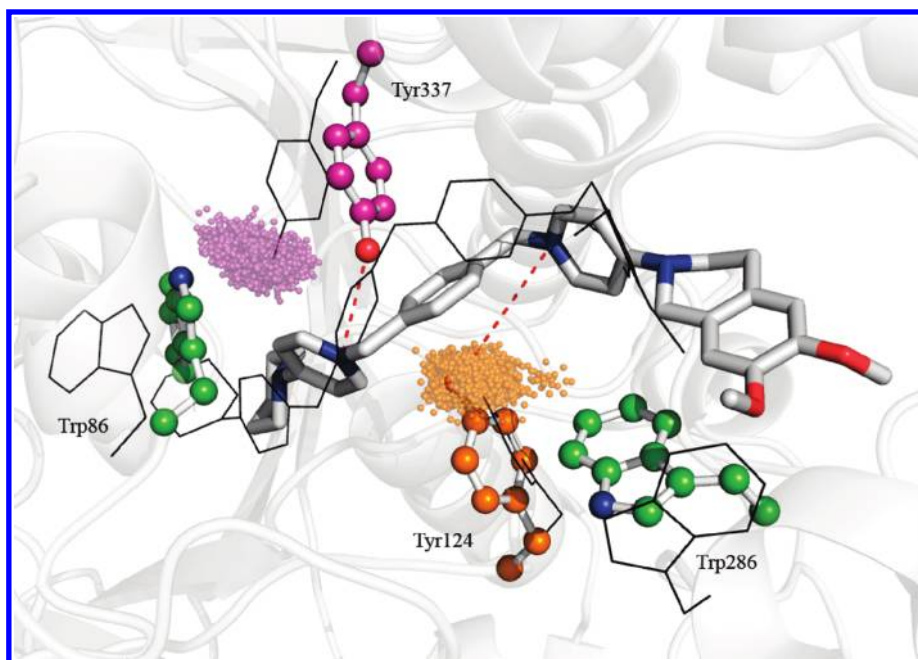


Figure 3. Top-scored docking pose of inhibitor **56** into *hAChE* (PDB code 1B41) is rendered in white capped stick models, while starting MD coordinates of residues Trp86 and Trp286 are in ball and stick models colored according to the standard atom code. The fitting spheres represent the positions visited during the 5 ns MD by the phenolic oxygen atoms of the nonconserved narrow gorge residues Tyr337 and Tyr124 and are colored in magenta and orange as the corresponding ball and stick models of their side chains. Black wireframe models indicate the amino acid side chain and inhibitor **56** conformations at the end of the 5 ns MD simulation. Red dashed lines show the occurrence of possible ion–dipole contacts established among the side chain oxygen atoms of Tyr337 and Tyr124 with the pyridinium nitrogen atoms at the distances of 4.82 (± 0.42) Å and 4.44 (± 0.35) Å, respectively.

hydrophobic and, taking into account the strong charge delocalization, cation– π interactions with Trp86 while, interestingly, a number of polar residues in the narrow spanning gorge, which are Tyr124, Tyr337, and to a lesser extent Asp74 and Tyr341, might engage polar interactions with the pyridinium nitrogens of the inhibitor. On the other side, the 6,7-dimethoxy-1,2,3,4-tetrahydroisoquinoline moiety was likely involved in hydrophobic interactions with the Trp286 of the PAS. The results acquired via docking simulations met those found in a previous study where the interactions of the 5,6-dimethoxy-indan-1-one moiety of donepezil in the peripheral binding site has been analyzed.³⁴ Incidentally, the docking of **56** in the *TcAChE* (PDB code 1EVE) did not return any significantly different binding mode (see Figure S3 in the Supporting Information).

Interestingly, the molecular docking of heterodimer **56** into BChE envisaged a less favorable GoldScore fitness value (-48 kJ/mol) for the top-scored docking pose presumably because of the lack of an efficient binding at the peripheral binding site in BChE. On the other hand, a detrimental effect on the affinity toward BChE might also be ascribed to the occurrence of some important residue mutations in the mid-gorge.³⁵ And indeed, two critical residues, Tyr124 and Tyr337 in *hAChE* were replaced with Gln119 and Ala328, respectively, in *hBChE*, and this might preclude the occurrence of the polar interactions in the mid-gorge previously pointed out. Molecular docking simulations nicely suggested a face-to-face interaction in the primary binding site between the Trp82 (BChE numbering) and inhibitor **56** as reported in a recent paper for other heterodimeric inhibitors^{11a} (see Figure S1 in the Supporting Information). Our prospective docking study finally addressed the complex formed between inhibitor **56** and ChoK. Basically, docking simulations predicted a prevalent binding mode showing the piperidinyl ring embedded

in a hydrophobic cavity of the catalytic site constituted by Tyr333, Tyr354, Tyr440, Trp420, Trp423, Phe362, and Phe435 (ChoK numbering).

For the sake of completeness, a series of molecular dynamic simulations were undertaken to retrospectively assess the structural integrity of the binding mode of **56** and, more importantly, to gain insight on the molecular reasons behind its selectivity toward AChE. To this end, two parallel 5 ns MD simulations were run on the complexes of **56** with *hAChE* and *hBChE*.

The top-scored docking poses were thus used as a convenient starting geometry for determining the structural variation over time of the AChE– and BChE–ligand complexes. Both systems were equilibrated according to standard MD protocols.³⁶ Satisfactorily, the visual inspection of the molecular frames obtained via MD unequivocally confirmed the correctness of the binding topology preliminarily predicted by docking in the stage of rational design. As far as the *hAChE*–ligand complex is concerned, the fundamental face-to-face interaction engaged with Trp86 at the primary binding site was very well conserved during the simulation, while the Trp286 at the PAS disclosed a weaker propensity to maintain the π – π stacking interaction with the 6,7-dimethoxy-1,2,3,4-tetrahydroisoquinoline of **56** observed in the docking study. And in fact, MD simulations showed that the average distance between the centroid of Trp86 and that of piperidinyl ring was equal to 4.69 (± 0.26) Å, and this was consistent with the hypothesis of a stable hydrophobic sandwich-like interaction. On the other hand, the larger average distance of 8.85 (± 1.01) Å, measured between the centroid of Trp286 and that of the 6,7-dimethoxy-1,2,3,4-tetrahydroisoquinoline, indicated only transient hydrophobic contacts at the PAS. Despite the likely disruption of such interaction at the PAS, the heterodimer **56** never did visit any alternative binding topology along

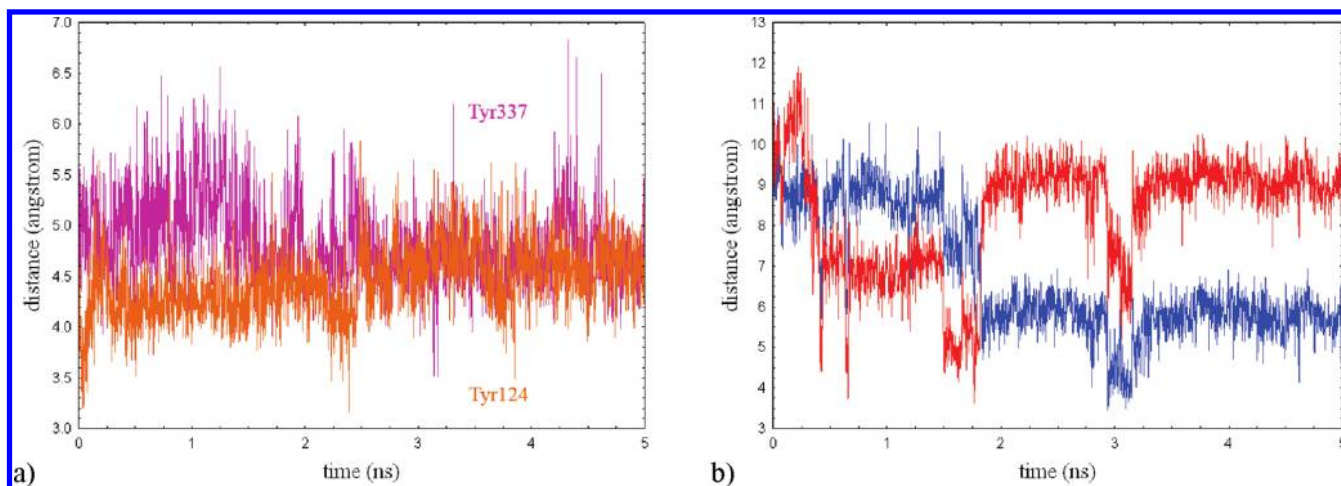


Figure 4. The left-hand side plot (a) shows the variation of the distance between the phenolic oxygen atoms of nonconserved Tyr337 and Tyr124 of *hAChE* (equivalent to Ala328 and Gln119 of *hBChE*) and the closest pyridinium nitrogen of compound **56** (the same color code of Figure 3 has been adopted). The right-hand side plot (b) shows the variation of the distances between the phenolic oxygen atoms of the conserved residue Tyr332 of *hBChE* (equivalent to Tyr341 of *hAChE*) and both the pyridinium nitrogen atoms of compound **56**. In particular, the red and blue profiles represent the distances to the charged nitrogen atoms of the pyridinium rings joined to the 6,7-dimethoxy-1,2,3,4-tetrahydroisoquinoline and the piperidine moieties, respectively. All the measures sampled during the 5 ns MD simulation are referenced to the two top-scored poses of **56** resulting from docking simulations into the binding sites of the two human ChEs.

the entire time of MD simulation. In this regard, nonconserved Tyr337 and Tyr124 residues of *hAChE* played an important role in stabilizing the binding mode of **56** by establishing ion–dipole interactions with both of the charged nitrogen atoms of the two pyridinium rings of **56**. As it can be inferred from Figure 4a, such interactions were maintained along all the MD, as the distances between the phenolic oxygen atoms of Tyr337 and Tyr124 and the corresponding closest charged nitrogen atom of the pyridinium rings changed within a very narrow range. More precisely, those distances were equal to $4.82 (\pm 0.42)$ Å and to $4.44 (\pm 0.35)$ Å, respectively. For a better understanding, the Cartesian positions of the phenolic oxygen atoms of the two tyrosine residues, sampled during the MD, were conveniently represented as fitting spheres, in Figure 3. Actually, the significant role of nonconserved mid-gorge residues (i.e., Tyr337 and Tyr124) of *hAChE* and their relevance in stabilizing the binding of **56** through a likely bidentate ion–dipole interaction with both the charged nitrogen atoms of the pyridinium rings were already observed in the docking studies. And this was observed despite the well-known preference of GoldScore scoring function to award hydrophobic rather than polar interactions.³⁷ On the other hand, the lack of a compact tyrosine-based network in the mid-gorge of *BChE* reduced by far the likeness of potential ion–dipole interactions. And in fact, MD simulation carried out on *BChE* assigned a secondary role to the conserved residue Tyr332 of *BChE* (equivalent to Tyr341 of *hAChE*). Such a residue acted like a switch, swapping between the two competing charged nitrogen atoms of the two pyridinium rings, in an attempt to find an optimal distance with at least one of them. Such a behavior is described in Figure 4b, which shows how the chance of finding an appropriate distance for establishing a ion–dipole interaction with one charged nitrogen atom was made at the expense of the other one. Retrospectively, MD simulations refined the preliminary hypothesis emerged in the step of rational molecular design via docking by furnishing a more convincing interpretation of the molecular selectivity

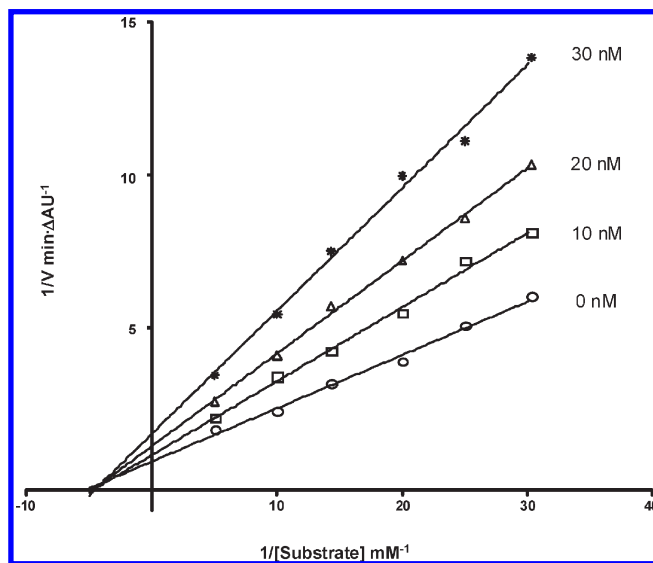


Figure 5. Lineweaver–Burk plot of inhibition kinetics of **56**: reciprocals of enzyme activity (bovine AChE) vs reciprocals of substrate (*S*-acetylthiocholine) concentration in the presence of different concentrations (0–30 nM) of inhibitor **56**.

with the recognition of the pivotal role of nonconserved residues of mid-gorge of *hAChE* in the binding of inhibitor **56**.

Heterodimer **56** was prepared (see Scheme 6) and tested as AChE, *BChE*, and ChoK inhibitors. Very gratifyingly, it exhibited an outstanding AChE affinity ($IC_{50} = 15$ nM) compared to *BChE* ($IC_{50} = 752$ nM), thus showing a high AChE selectivity ($SI = 50$) and being the most potent and selective AChE inhibitor of the whole series of examined molecules. Moreover, it showed very poor ChoK inhibitory potency ($IC_{50} = 8.43$ μ M), resulting in an excellent selectivity index ($SI = 562$).

The mechanism of AChE inhibition by **56** was assessed by means of a kinetic study whose results are reported in Figure 5.

This study accounted for a mixed-type model of inhibition, in accordance with a likely dual binding site mode of interaction,³⁴ with an apparent inhibition constant K_i equal to 21 ± 3 nM.

Finally, a further study was undertaken on a selected number of inhibitors to determine their inhibitory activity on the human isoforms of both ChEs and on the $A\beta_{1-40}$ self-aggregation. Along with **56**, three compounds were chosen as representatives of the different structural classes presented in Tables 1–4. Taking into account the diversity of the linkers, we selected the very potent AChE inhibitors **14** and **19**, bearing respectively a *p*-xylenyl and a 3,3'-biphenyl spacer, and the highly BChE-selective compound **47**. IC_{50} on human recombinant acetylcholinesterase and human serum butyrylcholinesterase and the percentage of inhibition of the $A\beta_{1-40}$ self-aggregation are reported in Table 5, along with the activities exhibited by two reference compounds, which are donepezil (AChE-selective) and tacrine (BChE-selective). Inhibition data of the two reference compounds are in agreement with literature data.^{38,39} The examined QASs exhibited an inhibitory potency toward the two human ChEs comparable to that observed for the bovine AChE and serum horse BChE. However, *h*AChE affinity and *h*AChE over *h*BChE selectivity of QAS **56** slightly decreased. The $A\beta_{1-40}$ antiaggregating activities of compounds in Table 5 at 100 μ M were very low, the most active compound being the QAS **19** with 30% ($\pm 2\%$) of inhibition.

CONCLUSION

The work described in the present paper was focused on the synthesis and biological evaluation as AChE and BChE inhibitors of a series of mono-, bis-, and tris-QASs. The application of molecular dimerization and hybridization approaches has laid the groundwork for the discovery of very active bis-QASs. Following this strategy, by connecting two cationic heads with a proper substitution pattern through a spacer of varying lipophilicity, length, and flexibility, we succeeded in obtaining a large number of compounds active in the nanomolar range, mainly as AChE inhibitors. A thorough analysis of the substituent effect in the cationic heads pointed out that the introduction of powerful electron-releasing groups modulated the affinity likely through a reinforcement of cation– π interaction and/or more favorable solvation/desolvation effects.¹³ Careful and stepwise structural modifications were made aiming at an improvement of the inhibitory potency toward AChE, the AChE over BChE selectivity, and even more importantly the AChE over ChoK selectivity. Very satisfactorily, our docking-assisted molecular design was very successful, leading to the discovery of compound **56**, the most active and selective AChE inhibitor of the whole examined series of compounds ($IC_{50} = 15$ nM, SI = 50). Moreover, compound **56** exhibited a quite poor ChoK inhibitory activity ($IC_{50} = 8.43 \pm 0.36$ μ M) resulting in an excellent selectivity index (SI = 562; SI is the $IC_{50}(\text{ChoK})/IC_{50}(\text{AChE})$ affinity ratio), and this was another important goal met in our study. Finally, the relevant AChE inhibitory potency, the favorable selectivity profile, and the high aqueous solubility and lipophilicity should guarantee for heterodimer **56** a prevalent activity at the peripheral level, strongly required in the therapy of MG and NMB.

EXPERIMENTAL SECTION

Chemistry. Starting materials, reagents, and analytical grade solvents were purchased from Sigma-Aldrich (Europe). Microwave reactions were performed in a Milestone MicroSynth apparatus, with setting of temperature and hold times, fixing of maximum irradiation

power to 500 W, and heating ramp times to 5 min. The purity of all the intermediates, checked by ^1H NMR and HPLC, was always better than 95%. Flash chromatographic separations were performed on Biotage SP1 purification system using flash cartridges prepacked with KP-Sil 32–63 μm , 60 Å silica. Except for those regarding final QASs compounds, reactions were routinely checked by TLC using Merck Kieselgel 60 F₂₅₄ aluminum plates and visualized by UV light or iodine. Melting points were determined by the capillary method on a Stuart Scientific SMP3 electrothermal melting point apparatus and are uncorrected. Elemental analyses were performed on the EuroEA 3000 analyzer only on the final compounds tested as ChEs inhibitors. The measured values for C, H, and N agreed to within $\pm 0.40\%$ of the theoretical values. Nuclear magnetic resonance spectra were recorded at 300 MHz on a Varian Mercury 300 instrument or 400 MHz ^1H and 100 MHz ^{13}C NMR Bruker ARX 400 or 300 MHz ^1H and 75 MHz ^{13}C NMR Bruker AMX-300 spectrometers or 400 MHz ^1H and 100 MHz ^{13}C NMR Varian NMR-System-TM 400 or 300 MHz ^1H and 75 MHz ^{13}C NMR Varian Inova spectrometers at ambient temperature. Chemical shifts (δ) are quoted in parts per million (ppm) and are referenced to the residual solvent peak. The following abbreviations were used: s (singlet), d (doublet), dd (doublet of doublet), t (triplet), pst (pseudotriplet), psq (pseudoquartet), q (quadruplet), m (multiplet), ddd (double doublet of doublet). Signals due to OH protons were located by deuterium exchange with D_2O . High-resolution liquid secondary ion mass spectra (HR LSIMS) were carried out on a VG AutoSpec Q high-resolution mass spectrometer (Fisons Instruments). All compounds were dried at 40 °C and 0.1 mmHg for 24 h, but many held on tenaciously to water which appear to be solvates. Compounds **7**,¹⁴ **8**,¹⁴ **11**,¹⁴ **13**,¹⁴ **14**,¹⁴ **17**–**19**,¹⁴ **23**–**26**,¹⁴ **29**,¹⁴ **30**,¹⁴ **31**,¹⁶ **32**,¹⁶ **33**–**35**,¹³ **37**,¹³ **38**–**40**,¹⁶ **45**,¹⁵ **46**,¹⁷ **51**,¹⁸ **52**,¹⁸ **53**,¹⁹ **54**,¹⁹ and **55**²⁰ were synthesized as previously reported. *trans*-1,2-Bis(hydroxymethyl)cyclopropane,²² *trans*-1,2-bis(bromomethyl)cyclopropane,²¹ 3,3'-bis(bromomethyl)biphenyl,²³ 4,4'-bis[(bromomethyl)biphenyl],²⁴ *trans,trans*-1,4-diphenyl-1,3-butadiene,²⁴ 1,4-bis[4-(bromomethyl)phenyl]butane,²⁴ *trans*-4,4'-bis(hydroxymethyl)stilbene,²⁶ and *trans*-4,4'-bis(bromomethyl)stilbene²⁵ were synthesized according to literature procedures. 4-(Morpholino)pyridine, 4-(dimethylamino)pyridine, 4-(pyrrolidino)pyridine, 4-aminoquinoline, biphenyl-4,4'-dicarboxylic acid, benzyl bromide, 4-methylbenzyl bromide, 1,3-bis(bromomethyl)benzene, 1,4-bis(bromomethyl)benzene, quinuclidine, and 3-quinuclidinol were purchased from commercial sources (Sigma-Aldrich, Europe).

Biphenyl-4,4'-dicarboxylic Acid Diethyl Ester (1a). Commercially available biphenyl-4,4'-dicarboxylic acid (9.7 g, 40.0 mmol) was suspended in ethanol (100 mL), and thionyl chloride (15 mL, 200 mmol) was slowly added. The reaction mixture was stirred at room temperature overnight and then refluxed for 24 h. After the mixture was cooled to room temperature, the solvent was evaporated under reduced pressure and the crude mixture was diluted with ethyl acetate (500 mL) and extracted with NaOH 2 N (3×100 mL). The organic phase was washed with brine (100 mL), dried over Na_2SO_4 , concentrated under vacuum, and finally purified by flash chromatography (gradient eluent, ethyl acetate in *n*-hexane 0% \rightarrow 10%), thus obtaining **1a** as a white solid. Yield: 52%. ^1H NMR (300 MHz, $\text{DMSO}-d_6$) δ : 1.33 (t, $J = 7.2$ Hz, 6H), 4.33 (q, $J = 7.2$ Hz, 4H), 7.88 (d, $J = 8.5$ Hz, 4H), 8.05 (d, $J = 8.5$ Hz, 4H).

(4'-Hydroxymethylbiphenyl-4-yl)methanol (1b). Ester **1a** (6.0 g, 20 mmol) was dissolved in dry THF (80 mL), and LiAlH_4 (3.0 g, 80 mmol) was added portionwise in 1 h. The mixture was refluxed for 7 h and then cooled to room temperature. Excess reducing agent was quenched by careful addition of water while cooling through an external ice bath. The mixture was kept under stirring for 15 min and extracted with chloroform (3×200 mL). The organic layers were collected, dried over Na_2SO_4 , and the solvent was removed under rotary evaporation. Final purification through flash chromatography (gradient eluent,

methanol in dichloromethane 0% → 5%) yielded intermediate **1b** as an off-white solid. Yield: 40%. ¹H NMR (300 MHz, DMSO-*d*₆) δ: 4.50 (d, *J* = 5.5 Hz, 4H), 5.18 (t, *J* = 5.5 Hz, 2H, dis. with D₂O), 7.36 (d, *J* = 8.3 Hz, 4H), 7.58 (d, *J* = 8.3 Hz, 4H).

4,4'-Bis(bromomethyl)biphenyl (1c). Carbon tetrabromide (2.7 g, 8.3 mmol) was added to a solution of **1b** (1.6 g, 7.5 mmol) in dry CH₂Cl₂ (50 mL). Triphenylphosphine (2.4 g, 9.0 mmol), previously dissolved in dry CH₂Cl₂ (20 mL), was added dropwise at 0 °C. The reaction mixture was slowly warmed to room temperature and then stirred for 6 h. After evaporation of the solvent, purification through flash chromatography (gradient eluent, ethyl acetate in *n*-hexane 0% → 10%) furnished derivative **1c**. Yield: 67%. ¹H NMR (300 MHz, DMSO-*d*₆) δ: 4.75 (s, 4H), 7.52 (d, *J* = 8.3 Hz, 4H), 7.66 (d, *J* = 8.3 Hz, 4H).

4-Piperidin-1-ylpyridine (1d). A Pyrex vessel was charged with a magnetic stirring bar, and then 4-chloropyridine hydrochloride (0.60 g, 4.0 mmol) was added and suspended in dry acetonitrile (10 mL). *N,N*-Diisopropylethylamine (2.1 mL, 12 mmol) was added followed by piperidine (0.40 mL, 4.0 mmol). The reactor was placed in a microwave apparatus and irradiated at 160 °C for 1 h. After cooling to room temperature, the mixture was partitioned between ethyl acetate (60 mL) and water (100 mL) and then extracted with ethyl acetate (3 × 60 mL). The organic layers were collected, washed with brine (50 mL), dried over Na₂SO₄, and then the solvent was removed under reduced pressure. Ether (5 mL) was added to the resulting crude oil, and the inorganic precipitate was filtered off. Evaporation of the solvent gave **1d** as a dark yellow solid of satisfactory purity, as confirmed by HPLC analysis. Yield: 82%. ¹H NMR (300 MHz, DMSO-*d*₆ + D₂O) δ: 1.48–1.61 (m, 6H), 3.29–3.32 (m, 4H), 6.74–6.76 (m, 2H), 8.07–8.10 (m, 2H).

2-Pyridin-4-yl-1,2,3,4-tetrahydroisoquinoline (1e). In a Pyrex vessel, charged with a magnetic stirring bar, a suspension of 1,2,3,4-tetrahydroisoquinoline hydrochloride (0.51 g, 3.0 mmol) and 4-chloropyridine hydrochloride (0.50 g, 3.3 mmol) in dry acetonitrile (10 mL) was prepared. *N,N*-Diisopropylethylamine (1.7 mL, 10 mmol) was added, and the reactor was introduced in a microwave apparatus and irradiated for 1 h at 160 °C. After cooling to room temperature, the mixture was poured onto ice (100 mL) and then extracted with ethyl acetate (3 × 60 mL). The organic layers were collected, washed with brine (50 mL), and dried over Na₂SO₄. The organic solution was then concentrated under reduced pressure and purified through flash chromatography (gradient eluent, methanol in acetone 0% → 5%), yielding **1e** as a yellow solid. Yield: 74%. ¹H NMR (300 MHz, DMSO-*d*₆) δ: 2.89 (t, *J* = 6.1 Hz, 2H), 3.59 (t, *J* = 6.1 Hz, 2H), 4.48 (s, 2H), 6.81–6.84 (m, 2H), 7.17–7.25 (m, 4H), 8.13–8.15 (m, 2H).

6,7-Dimethoxy-2-pyridin-4-yl-1,2,3,4-tetrahydroisoquinoline (1f). In a Pyrex vessel, charged with a magnetic stirring bar, a suspension of 6,7-dimethoxy-1,2,3,4-tetrahydroisoquinoline hydrochloride (0.69 g, 3.0 mmol) and 4-chloropyridine hydrochloride (0.50 g, 3.3 mmol) in dry acetonitrile (10 mL) was prepared. *N,N*-Diisopropylethylamine (1.7 mL, 10 mmol) was added, and the reactor was introduced in a microwave apparatus and irradiated for 1 h at 160 °C. After cooling to room temperature, the mixture was poured onto crushed ice (150 g) and the resulting solid was filtered and washed with water, thus obtaining **1f** as an off-white solid. Yield: 78%. ¹H NMR (300 MHz, DMSO-*d*₆) δ: 2.79 (t, *J* = 5.8 Hz, 2H), 3.57 (t, *J* = 5.8 Hz, 2H), 3.70 (s, 3H), 3.71 (s, 3H), 4.39 (s, 2H), 6.76–6.82 (m, 4H), 8.13 (d, *J* = 5.5 Hz, 2H).

4-Cyclohexylpyridine (1g). Magnesium turnings (0.21 g, 8.8 mmol) were suspended in dry diethyl ether (3.0 mL) in a flame-dried round-bottom flask equipped with a reflux condenser. While the mixture was being stirred, the solvent was evaporated under reduced pressure. The system was purged under argon stream for 10 min. This procedure was repeated twice, and then the flask was gently heated under vacuum for 10 min. The system was again purged through an argon stream for

10 min. Then a volume of 2.0 mL of dry THF was introduced, followed by the dropwise addition of a solution of iodine (catalytic amount) in dry THF (4.0 mL) and finally of cyclohexyl bromide (0.99 mL, 8.0 mmol). When the dark brown color of the solution disappeared and turned to a gray suspension, the mixture was refluxed for 1 h. After the mixture was cooled to room temperature, the Grignard reagent was added dropwise through a syringe under an argon atmosphere to a solution of 4-chloropyridine¹³ (0.60 g, 5.3 mmol), Fe(acac)₃ (0.19 g, 0.53 mmol), and NMP (0.85 mL) in dry THF (11.0 mL) while the mixture cooled to 0 °C. The reaction mixture turned red and then was stirred at room temperature. After 15 h, water (150 mL) was added and the mixture was extracted with diethyl ether (3 × 60 mL). The organic layers were collected, dried over Na₂SO₄, and then the mixture was kept under an argon stream until evaporation of the solvent and disappearance of the spot of low-boiling 4-chloropyridine from the TLC control. In this way, 4-cyclohexylpyridine **1g** was obtained as a dark yellow oil as confirmed by ¹H NMR analysis and with a purity higher than 95% as checked by HPLC. Yield: 41%. ¹H NMR (300 MHz, DMSO-*d*₆) δ: 0.73–0.83 (m, 1H), 1.15–1.27 (m, 2H), 1.32–1.40 (m, 4H), 1.66–1.71 (m, 1H), 1.75–1.78 (m, 2H), 2.42–2.51 (m, 1H), 7.22 (d, *J* = 6.1 Hz, 2H), 8.42 (d, *J* = 6.1 Hz, 2H).

4-Phenylpyridine (1h). 4-Bromopyridine hydrochloride (0.39 g, 2.0 mmol) and phenylboronic acid (0.29 g, 2.4 mmol) were suspended in a dimethoxyethane/water 4/1 (v/v) mixture (15 mL). Cs₂CO₃ was added (1.3 g, 4.0 mmol) followed by Pd(PPh₃)₄ (0.23 g, 0.2 mmol). The reaction mixture was heated to 80 °C for 4 h, and then DME was evaporated under vacuum. The mixture was partitioned between water (50 mL) and ether (200 mL), and then the organic phase was washed with a saturated aqueous solution of Na₂CO₃ (3 × 80 mL), dried over Na₂SO₄, and concentrated to dryness by rotary evaporation. Purification by flash chromatography (gradient eluent, ethyl acetate in *n*-hexane 0% → 40%) yielded **1h** as a white solid. Yield: 93%. ¹H NMR (300 MHz, DMSO-*d*₆) δ: 7.46–7.54 (m, 3H), 7.70 (d, *J* = 6.3 Hz, 2H), 7.77–7.81 (m, 2H), 8.63 (d, *J* = 6.3 Hz, 2H).

General Procedure for the Preparation of Mono- and Bis-pyridinium Bromides 2–6, 9, 10, 12, 15, 16, 20–22, 27, 28, 36, 41–44, and 47–50. A solution of the appropriate bromomethyl or bis(bromomethyl) linker and the appropriate 4-substituted pyridine (in a 1:1 or a 1:2 molar ratios) was heated to 100 °C in a sealed tube in 2-butanone (4.0 mL) from 15 to 192 h on a 0.2 mmol scale. After filtration and thorough washing with 2-butanone, ethyl acetate, and diethyl ether, the solid was purified by recrystallization from ethanol or methanol after adding diethyl ether to turbidity.

1-Benzyl-4-(pyrrolidin-1-yl)pyridinium Bromide (2). White solid. Yield: 27%. Mp: 227–229 °C. ¹H NMR (300 MHz, CD₃OD) δ: 2.11 (m, 4H), 3.55 (m, 4H), 5.37 (s, 2H), 6.87 (d, *J* = 7.8 Hz, 2H), 7.41 (m, 5H), 8.21 (d, *J* = 7.8 Hz, 2H). HR LSIMS (*m/z*) calcd for C₁₆H₁₉N₂ (M-Br)⁺ 239.1543; found 239.1545. Anal. (C₁₆H₁₉BrN₂·0.5H₂O) C, H, N.

1-(4-Methylbenzyl)-4-(pyrrolidin-1-yl)pyridinium Bromide (3). White solid. Yield: 87%. Mp: 188–190 °C. ¹H NMR (400 MHz, CD₃OD) δ: 2.11 (psq, *J* = 6.7 Hz, 4H), 2.33 (s, 3H), 3.54 (pst, *J* = 6.7 Hz, 4H), 5.31 (s, 2H), 6.85 (d, *J* = 7.5 Hz, 2H), 7.23 (d, *J* = 8.1 Hz, 2H), 7.28 (d, *J* = 8.1 Hz, 2H), 8.20 (d, *J* = 7.5 Hz, 2H). HR LSIMS (*m/z*) calcd for C₁₇H₂₁N₂ (M - Br)⁺ 253.1705; found 253.1698. Anal. (C₁₇H₂₁BrN₂·0.7H₂O) C, H, N.

4-Amino-1-(4-methylbenzyl)quinolinium Bromide (4). White solid. Yield: 71%. Mp: 261–263 °C. ¹H NMR (400 MHz, CD₃OD) δ: 2.29 (s, 3H), 5.75 (s, 2H), 6.92 (d, *J* = 7.3 Hz, 1H), 7.13 (d, *J* = 8.2 Hz, 2H), 7.17 (d, *J* = 8.2 Hz, 2H), 7.68 (pst, *J* = 7.7 Hz, 1H), 7.90 (pst, *J*₁ = 1.2 Hz, *J*₂ = 6.9 Hz, *J*₃ = 8.6 Hz, 1H), 7.98 (d, *J* = 8.8 Hz, 1H), 8.40 (d, *J* = 8.4 Hz, 1H), 8.58 (d, *J* = 7.3 Hz, 1H). HR LSIMS (*m/z*) calcd for C₁₇H₁₇N₂ (M - Br)⁺ 249.1392; found 249.1398. Anal. (C₁₇H₁₇BrN₂·0.2H₂O) C, H, N.

1,1'-[trans-Cyclopropane-1,2-diylbis(methylene)]bis(4-(dimethylamino)pyridinium Dibromide (5). White solid. Yield: 62%. Mp: 284–5 °C. ¹H NMR (300 MHz, CD₃OD) δ: 0.98 (t, J = 6.7 Hz, 2H), 1.66–1.68 (m, 2H), 3.26 (s, 12H), 3.93 (dd, *J*_{vic} = 8.1 Hz, *J*_{gem} = 14.1 Hz, 2H), 4.29 (dd, *J*_{vic} = 5.8 Hz, *J*_{gem} = 14.1 Hz, 2H), 6.65 (d, *J* = 7.7 Hz, 4H), 8.19 (d, *J* = 7.7 Hz, 4H). HR LSIMS (*m/z*) calcd for C₁₉H₂₈Br₂N₄Na (M + Na)⁺ 493.0578; found 493.0580. Anal. (C₁₉H₂₈Br₂N₄ · 1.5H₂O) C, H, N.

1,1'-[1,3-Phenylenebis(methylene)]bis[4-(dimethylamino)pyridinium] Dibromide (6). Off-white solid. Yield: 64%. Mp > 300 °C. ¹H NMR (300 MHz, CD₃OD) δ: 3.26 (s, 12H), 5.43 (s, 4H), 7.04 (d, *J* = 7.7 Hz, 4H), 7.52–7.39 (m, 3H), 7.57 (s, 1H), 8.28 (d, *J* = 7.7 Hz, 4H). HR LSIMS (*m/z*) calcd for C₂₂H₂₈Br₂N₄Na (M + Na)⁺ 529.0578; found 529.0576. Anal. (C₂₂H₂₈Br₂N₄ · 0.5H₂O) C, H, N.

1,1'-[1,3-Phenylenebis(methylene)]bis[4-(3,4-dihydroisoquinolin-2(1*H*)-yl)pyridinium] Dibromide (9). Yellow solid. Yield: 69%. Mp: 128–130 °C (dec). ¹H NMR (300 MHz, CD₃OD) δ: 3.06 (t, *J* = 6.1 Hz, 4H), 3.82 (t, *J* = 6.1 Hz, 4H), 4.77 (s, 4H), 5.42 (s, 4H), 7.20–7.26 (m, 12H), 7.37–7.52 (m, 4H), 8.30 (d, *J* = 7.2 Hz, 4H). Anal. (C₃₆H₃₆Br₂N₄ · 2H₂O) C, H, N.

1,1'-[1,3-Phenylenebis(methylene)]bis[4-(6,7-dimethoxy-3,4-dihydroisoquinolin-2(1*H*)-yl)pyridinium] Dibromide (10). Yellow solid. Yield: 51%. Mp: 261–263 °C. ¹H NMR (300 MHz, CD₃OD) δ: 2.95 (t, *J* = 6.1 Hz, 4H), 3.78 (t, *J* = 6.1 Hz, 4H), 3.80 (s, 12H), 4.66 (s, 4H), 5.42 (s, 4H), 6.83 (s, 2H), 6.87 (s, 2H), 7.21 (d, *J* = 6.8 Hz, 4H), 7.42–7.50 (m, 4H), 8.29 (d, *J* = 6.8 Hz, 4H). Anal. (C₄₀H₄₄Br₂N₄O₄ · 1.5H₂O) C, H, N.

1,1'-[1,4-Phenylenebis(methylene)]bis[4-(dimethylamino)pyridinium] Dibromide (12). White solid. Yield: 51%. Mp > 300 °C. ¹H NMR (400 MHz, CD₃OD) δ: 3.25 (s, 12H), 5.40 (s, 4H), 7.01 (d, *J* = 7.9 Hz, 4H), 7.46 (s, 4H), 8.23 (d, *J* = 7.9 Hz, 4H). HR LSIMS (*m/z*) calcd for C₂₂H₂₈Br₂N₄ (M – Br)⁺ 427.1497; found 427.1494. Anal. (C₂₂H₂₈Br₂N₄) C, H, N.

1,1'-[1,4-Phenylenebis(methylene)]bis[4-(3,4-dihydroisoquinolin-2(1*H*)-yl)pyridinium] Dibromide (15). Off-white solid. Yield: 55%. Mp: 78–80 °C (dec). ¹H NMR (300 MHz, D₂O) δ: 2.34 (t, *J* = 5.8 Hz, 4H), 3.03 (t, *J* = 5.8 Hz, 4H), 3.76 (s, 4H), 5.17 (s, 4H), 6.28 (d, *J* = 7.4 Hz, 4H), 6.48–6.53 (m, 4H), 6.64–6.67 (m, 2H), 6.71–6.76 (m, 2H), 7.52 (s, 4H), 7.96 (d, *J* = 7.4 Hz, 4H). Anal. (C₃₆H₃₆Br₂N₄ · 2H₂O) C, H, N.

1,1'-[1,4-Phenylenebis(methylene)]bis[4-(6,7-dimethoxy-3,4-dihydroisoquinolin-2(1*H*)-yl)pyridinium] Dibromide (16). Off-white solid. Yield: 68%. Mp: 157–159 °C (dec). ¹H NMR (300 MHz, CD₃OD) δ: 2.97 (t, *J* = 5.8 Hz, 4H), 3.81 (t, *J* = 5.8 Hz, 4H), 3.82 (s, 6H), 3.83 (s, 6H), 4.69 (s, 4H), 5.41 (s, 4H), 6.85 (s, 2H), 6.87 (s, 2H), 7.21 (d, *J* = 6.6 Hz, 4H), 7.46 (s, 4H), 8.27 (d, *J* = 6.6 Hz, 4H). Anal. (C₄₀H₄₄Br₂N₄O₄ · 2H₂O) C, H, N.

1,1'-[Biphenyl-3,3'-diylbis(methylene)]bis(4-cyclohexylpyridinium) Dibromide (20). Off-white solid. Yield: 48%. Mp: 244–246 °C. ¹H NMR (300 MHz, CD₃OD) δ: 1.31–1.42 (m, 2H), 1.46–1.55 (m, 8H), 1.78–1.82 (m, 2H), 1.88–2.01 (m, 8H), 2.86–2.93 (m, 2H), 5.85 (s, 4H), 7.49–7.59 (m, 4H), 7.74–7.78 (m, 2H), 7.95–7.96 (m, 2H), 7.99 (d, *J* = 6.9 Hz, 4H), 9.49 (d, *J* = 6.9 Hz, 4H). Anal. (C₃₆H₄₂Br₂N₂ · 2H₂O) C, H, N.

1,1'-[Biphenyl-3,3'-diylbis(methylene)]bis(4-phenylpyridinium) Dibromide (21). Off-white solid. Yield: 73%. Mp: 156–158 °C. ¹H NMR (300 MHz, CD₃OD) δ: 5.92 (s, 4H), 7.57–7.64 (m, 10H), 7.78–7.81 (m, 2H), 7.98–8.00 (m, 6H), 8.42 (d, *J* = 6.9 Hz, 4H), 9.12 (d, *J* = 6.9 Hz, 4H). Anal. (C₃₆H₃₀Br₂N₂ · H₂O).

1,1'-[Biphenyl-3,3'-diylbis(methylene)]bis[4-(6,7-dimethoxy-3,4-dihydroisoquinolin-2(1*H*)-yl)pyridinium] Dibromide (22). Yellow solid. Yield: 63%. Mp: 164 °C (dec), 250–251 °C. ¹H NMR (300 MHz, CD₃OD) δ: 2.96 (t, *J* = 6.0 Hz, 4H), 3.80 (s, 6H), 3.81 (s, 6H), 3.82 (t, *J* = 6.0 Hz, 4H), 4.69 (s, 4H), 5.47 (s, 4H), 6.84 (s, 2H), 6.87

(s, 2H), 7.22 (d, *J* = 6.7 Hz, 4H), 7.38–7.41 (m, 2H), 7.49–7.55 (m, 2H), 7.67–7.69 (m, 2H), 7.78 (s, 2H), 8.36 (d, *J* = 6.7 Hz, 4H). Anal. (C₄₆H₄₈Br₂N₄O₄ · 2.5H₂O) C, H, N.

1,1'-[Biphenyl-4,4'-diylbis(methylene)]bis[4-(3,4-dihydroisoquinolin-2(1*H*)-yl)pyridinium] Dibromide (27). Yellow solid. Yield: 62%. Mp: 88–91 °C (dec). ¹H NMR (300 MHz, CD₃OD) δ: 3.06 (t, *J* = 6.1 Hz, 4H), 3.83 (t, *J* = 6.1 Hz, 4H), 4.77 (s, 4H), 5.44 (s, 4H), 7.26–7.29 (m, 12H), 7.47–7.49 (m, 4H), 7.68–7.71 (m, 4H), 8.31 (d, *J* = 7.2 Hz, 4H). Anal. (C₄₂H₄₀Br₂N₄ · 2.5H₂O) C, H, N.

1,1'-[Biphenyl-4,4'-diylbis(methylene)]bis[4-(6,7-dimethoxy-3,4-dihydroisoquinolin-2(1*H*)-yl)pyridinium] Dibromide (28). Yellow solid. Yield: 43%. Mp: 224–225 °C (dec). ¹H NMR (300 MHz, CD₃OD) δ: 2.98 (t, *J* = 5.8 Hz, 4H), 3.81–3.84 (m, 16H), 4.70 (s, 4H), 5.43 (s, 4H), 6.85 (s, 2H), 6.87 (s, 2H), 7.23 (d, *J* = 6.9 Hz, 4H), 7.48 (d, *J* = 8.0 Hz, 4H), 7.70 (d, *J* = 8.0 Hz, 4H), 8.30 (d, *J* = 6.9 Hz, 4H). Anal. (C₄₆H₄₈Br₂N₄O₄ · 2H₂O) C, H, N.

1,1'-[4,4'-(Ethane-1,2-diyl)bis(4,1-phenylene)]bis(methylene)bis(4-morpholinopyridinium) Dibromide (36). Off-white solid. Yield: 100%. Mp: 180–182 °C. ¹H NMR (300 MHz, CD₃OD) δ: 2.90 (s, 4H), 3.70 (t, *J* = 4.5 Hz, 8H), 3.80 (t, *J* = 4.5 Hz, 8H), 5.36 (s, 4H), 7.19 (d, *J* = 7.9 Hz, 4H), 7.23 (d, *J* = 8.2 Hz, 4H), 7.32 (d, *J* = 8.2 Hz, 4H), 8.29 (d, *J* = 7.9 Hz, 4H). HR LSIMS (*m/z*) calcd for C₃₄H₄₀Br₂N₄O₂ (M – Br)⁺ 615.2335; found 615.2335. Anal. (C₃₄H₄₀Br₂N₄O₂ · 1.5H₂O) C, H, N.

1,1'-[4,4'-(Butane-1,4-diyl)bis(1,4-phenylene)]bis(methylene)bis(4-(dimethylamino)pyridinium) Dibromide (41). Off-white solid. Yield: 89%. Mp: 161–163 °C. ¹H NMR (300 MHz, CD₃OD) δ: 1.70 (m, 4H), 2.72 (t, 4H), 3.33 (s, 12H), 5.42 (s, 4H), 7.09 (d, *J* = 7.9 Hz, 4H), 7.31 (d, *J* = 8.2 Hz, 4H), 7.39 (d, *J* = 8.2 Hz, 4H), 8.32 (d, *J* = 7.9 Hz, 4H). HR LSIMS (*m/z*) calcd for C₃₂H₄₀Br₂N₄ (M – Br)⁺ 559.2431; found 559.2429. Anal. (C₃₂H₄₀Br₂N₄ · 1.2H₂O) C, H, N.

1,1'-[4,4'-(Butane-1,4-diyl)bis(1,4-phenylene)]bis(methylene)bis[4-(pyrrolidin-1-yl)pyridinium] Dibromide (42). Off-white solid. Yield: 67%. Mp: 107–109 °C. ¹H NMR (300 MHz, CD₃OD) δ: 1.61 (m, 4H), 2.11 (m, 8H), 2.63 (m, 4H), 3.55 (m, 8H), 5.32 (s, 4H), 6.86 (d, *J* = 7.8 Hz, 4H), 7.22 (d, *J* = 8.2 Hz, 4H), 7.30 (d, *J* = 8.2 Hz, 4H), 8.20 (d, *J* = 7.8 Hz, 4H). HR LSIMS (*m/z*) calcd for C₃₆H₄₄Br₂N₄ (M – Br)⁺ 611.2744; found 611.2747. Anal. (C₃₆H₄₄Br₂N₄ · 2.5H₂O) C, H, N.

1,1'-[4,4'-(Butane-1,4-diyl)bis(1,4-phenylene)]bis(methylene)bis[4-(piperidin-1-yl)pyridinium] Dibromide (43). White solid. Yield: 60%. Mp: 259–261 °C. ¹H NMR (300 MHz, CD₃OD) δ: 1.65–1.81 (m, 16H), 2.67 (m, 4H), 3.71–3.75 (m, 8H), 5.33 (s, 4H), 7.15 (d, *J* = 7.9 Hz, 4H), 7.25 (d, *J* = 8.4 Hz, 4H), 7.33 (d, *J* = 8.4 Hz, 4H), 8.20 (d, *J* = 7.5 Hz, 4H). HR LSIMS (*m/z*) calcd for C₃₈H₄₇N₄ (M – HBr – Br)⁺ 559.3801; found 559.3803. Anal. C₃₈H₄₈Br₂N₄ · 2H₂O) C, H, N.

(E)-1,1'-[4,4'-(Ethene-1,2-diyl)bis(1,4-phenylene)]bis(methylene)bis[4-(piperidin-1-yl)pyridinium] Dibromide (44). White solid. Yield: 84%. Mp > 300 °C. ¹H NMR (400 MHz, CD₃OD) δ: 1.70–1.77 (m, 12H), 3.68–3.71 (m, 8H), 5.34 (s, 4H), 7.13 (d, *J* = 7.5 Hz, 4H), 7.23 (s, 2H), 7.39 (d, *J* = 7.8 Hz, 4H), 7.63 (d, *J* = 7.8 Hz, 4H), 8.19 (d, *J* = 7.8 Hz, 4H). HR LSIMS (*m/z*) calcd for C₃₆H₄₂Br₂N₄Na (M + Na)⁺ 711.1674; found 711.1665. Anal. (C₃₆H₄₂Br₂N₄ · 1.8H₂O) C, H, N.

1,1'-[Biphenyl-3,3'-diylbis(methylene)]bis(quinuclidinium) Dibromide (47). White solid. Yield: 84%. Mp > 300 °C. ¹H NMR (300 MHz, CD₃OD) δ: 1.98–2.10 (m, 12H), 2.17–2.20 (m, 2H), 3.59–3.64 (m, 12H), 4.59 (s, 4H), 7.58 (d, *J* = 7.9 Hz, 2H), 7.66 (t, *J* = 7.7 Hz, 2H), 7.48 (d, *J* = 7.5 Hz, 2H), 8.01 (s, 2H). HR LSIMS (*m/z*) calcd for C₂₈H₃₈Br₂N₂ (M – Br)⁺ 481.2218; found 481.2219. Anal. (C₂₈H₃₈Br₂N₂ · 2H₂O) C, H, N.

1,1'-[Biphenyl-3,3'-diylbis(methylene)]bis(3-hydroxyquinuclidinium) Dibromide (48). White solid. Yield: 76%. Mp > 300 °C. ¹H NMR (300 MHz, CD₃OD) δ: 1.85–1.94 (m, 4H), 2.08–2.20

(m, 4H), 2.31–2.36 (m, 2H), 3.25–3.30 (m, 2H), 3.44–3.67 (m, 8H), 3.85–3.92 (m, 2H), 4.23–4.26 (m, 2H), 4.63 (m, 4H), 7.48 (d, $J = 7.5$ Hz, 2H), 7.66 (t, $J = 7.7$ Hz, 2H), 7.90 (d, $J = 7.5$ Hz, 2H), 8.02 (s, 2H). HR LSIMS (m/z) calcd for $C_{28}H_{37}N_2O_2$ ($M - HBr - Br$)⁺ 433.2855; found 433.2852. Anal. ($C_{28}H_{38}Br_2N_2O_2 \cdot 1.6H_2O$) C, H, N.

1,1'-[4,4'-(Ethane-1,2-diyl)bis(1,4-phenylene)]bis(methylene)bis(3-hydroxyquinuclidinium) Dibromide (49). White solid. Yield: 53%. Mp: 274–276 °C. ¹H NMR (300 MHz, CD₃OD) δ : 1.78–1.97 (m, 4H), 2.05 (m, 2H), 2.22–2.35 (m, 2H), 2.29 (m, 2H), 3.00 (s, 4H), 3.11 (ddd, $J_1 = 2.5$ Hz, $J_2 = 3.0$ Hz, $J_3 = 13.0$ Hz, 2H), 3.31–4.49 (m, 8H), 3.71 (ddd, $J_1 = 3.0$ Hz, $J_2 = 8.3$ Hz, $J_3 = 13.0$ Hz, 2H), 4.18–4.20 (m, 2H), 4.38 (d, $J = 13.0$ Hz, 2H), 4.44 (d, $J = 13.0$ Hz, 2H), 7.33 (d, $J = 8.3$ Hz, 4H), 7.42 (d, $J = 8.3$ Hz, 4H). HR LSIMS (m/z) calcd for $C_{30}H_{42}Br_2N_2O_2$ ($M - Br$)⁺ 541.2424; found 541.2419. Anal. ($C_{30}H_{42}Br_2N_2O_2 \cdot 1H_2O$) C, H, N.

(E)-1,1'-[4,4'-(Ethene-1,2-diyl)bis(1,4-phenylene)]bis(methylene)bis(3-hydroxyquinuclidinium) Dibromide (50). Off-white solid. Yield: 39%. Mp 153–155 °C. ¹H NMR (400 MHz, CD₃OD) δ : 1.81–1.96 (m, 4H), 2.07 (m, 2H), 2.16–2.18 (m, 2H), 2.25–2.35 (m, 2H), 3.13 (d, $J = 12.9$ Hz, 2H), 3.33–3.52 (m, 8H), 3.73 (m, 2H), 4.19–4.21 (m, 2H), 4.40 (d, $J = 12.9$ Hz, 2H), 4.45 (d, $J = 12.9$ Hz, 2H), 6.77 (s, 2H), 7.36 (d, $J = 8.2$ Hz, 4H), 7.43 (d, $J = 8.2$ Hz, 4H). HR LSIMS (m/z) calcd for $C_{30}H_{40}Br_2N_2O_2$ ($M - Br$)⁺ 539.2268; found 539.2271. Anal. ($C_{30}H_{40}Br_2N_2O_2 \cdot 2.2H_2O$) C, H, N.

1-[4-(Bromomethyl)benzyl]-4-piperidin-1-ylpyridinium Bromide (1i). 1,4-Bis(bromomethyl)benzene (0.11 g, 0.40 mmol) was stirred in 2-butanone (3.5 mL) until complete dissolution, and **1d** (0.026 g, 0.16 mmol), previously dissolved in butanone (0.5 mL), was added in 5 portions of 0.10 mL each, within 96 h during which the mixture was heated to 100 °C. Then stirring and heating were continued for an additional 24 h, and the mixture was cooled to room temperature and washed with butanone and diethyl ether, yielding monobromide **1i** as an off-white solid. Yield: 89%. ¹H NMR (300 MHz, CD₃OD) δ : 1.70–1.77 (m, 6H), 3.68–3.72 (m, 4H), 4.57 (s, 2H), 5.32 (s, 2H), 7.12 (d, $J = 7.7$ Hz, 2H), 7.35 (d, $J = 8.3$ Hz, 2H), 7.48 (d, $J = 8.3$ Hz, 2H), 8.16 (d, $J = 7.7$ Hz, 2H).

4-(6,7-Dimethoxy-3,4-dihydroisoquinolin-2(1H)-yl)-1-[4-(4-piperidin-1-ylpyridinium-1-yl)methyl]benzyl]pyridinium Dibromide (56). Intermediate **1i** (0.043 g, 0.10 mmol) was suspended in a 2-butanone/acetonitrile 4/1 (v/v) mixture (4.0 mL), and **1f** (0.27 g, 0.10 mmol) was added. The mixture was refluxed for 48 h. After the mixture was cooled, the solid was washed with 2-butanone, acetonitrile, and ethanol, giving an off-white solid that was recrystallized from ethanol/diethyl ether, yielding an off-white solid. Yield: 75%. Mp: 134–136 °C (dec), 194–196 °C. ¹H NMR (300 MHz, CD₃OD) δ : 1.70–1.78 (m, 6H), 2.98 (t, $J = 5.8$ Hz, 2H), 3.68–3.72 (m, 4H), 3.80–3.84 (m, 8H), 4.70 (s, 2H), 5.35 (s, 2H), 5.41 (s, 2H), 6.85 (s, 1H), 6.87 (s, 1H), 7.12 (d, $J = 7.4$ Hz, 2H), 7.22 (d, $J = 7.4$ Hz, 2H), 7.46 (s, 4H), 8.16 (d, $J = 7.4$ Hz, 2H), 8.27 (d, $J = 7.4$ Hz, 2H). Anal. ($C_{34}H_{40}Br_2N_4O_2 \cdot 2H_2O$) C, H, N.

Molecular Modeling. GOLD (version 4.1.2), a genetic algorithm based software, was used for the docking study. GoldScore and ChemScore were used as fitness functions to rank the docking simulations on ChEs and ChoK, respectively. GoldScore is made up of four components that account for protein–ligand binding energy: protein–ligand hydrogen bond energy, protein–ligand van der Waals energy, ligand internal van der Waals energy, and ligand torsional strain energy. ChemScore was instead derived empirically from a set of 82 protein–ligand complexes for which measured binding affinities were available. ChemScore estimates the total free energy change that occurs on ligand binding by accounting for a number of physical contributions to free energy (e.g., hydrogen bonding) whose weight is determined by regression. Parameters used in the fitness function (e.g., hydrogen bond energies, atom radii and polarizabilities, torsion potentials, and hydrogen

bond directionalities) were taken from the GOLD parameter file. In the present study, the 3D coordinates of hAChE (PDB code 1B41), hBChE (PDB code 1P0I), TcAChE (PDB code 1EVE), and hChoK (PDB code 3F2R) were retrieved from the Protein Data Bank. The target proteins were prepared by adding hydrogen atoms, completing and optimizing missing residues, and removing water and cocrystallized molecules. As is well-known,⁴⁰ the histidine side chains cannot normally be placed into the electron density map unambiguously. As a result, the protonation state of such residues was adjusted according to the formation of HB networks that was further confirmed upon visual inspection. The basic amino functional groups were protonated. Aromatic amino functional groups were left uncharged, and carboxylic groups were considered to be deprotonated. Molecular docking on human AChE and ChoK resulted in 10 poses per inhibitor in a sphere of 10 and 15 Å radius centered on the centroid atom of donepezil (cocrystallized with TcAChE, PDB code 1EVE, previously aligned to hAChE) and of hemicholinium-3, respectively.

Molecular Dynamics. The top-scored solution from molecular docking of compound **56** was used as the initial enzyme–inhibitor complex for MD simulations. hAChE– and hBChE–**56** complexes were immersed in a cubic TIP3P water box that extended 18 Å from the protein surface atoms. The system was neutralized by addition of Na⁺ counterions using the AMBER Leap module. This led to a total of 108 129 atoms and of 107 934 for the hAChE– and hBChE–**56** complexes, respectively. The parm03 version of the all-atom AMBER force field was used to model the system. Solvent molecules were initially relaxed by means of energy minimizations and 30 ps of MD. Subsequently, the full system was minimized to remove bad contacts in the initial geometry and heated gradually to 310 K during 600 ps of MD. The SHAKE algorithm was employed to constrain all R–H bonds, and periodic boundary conditions were applied to simulate a continuous system. A nonbonded cutoff of 12 Å was used, whereas the particle mesh Ewald (PME) method was employed to include the contributions of long-range interactions. The pressure (1 atm) and the temperature (310 K) of the system were controlled by the Langevin thermostat–barostat via NAMD, the software used for the 5 ns MD simulations. The time-step was 1.5 fs, and the system was simulated for a total of 5 ns, with coordinates saved every 2 ps.

Cholinesterase Inhibition. The in vitro inhibition assays of AChE from bovine erythrocytes (0.36 U/mg) and BChE from equine serum (13 U/mg) were run in phosphate buffer 0.1 M, at pH 8.0. Acetyl- and butyrylthiocholine iodides were used, respectively, as substrates, and 5,5'-dithiobis(2-nitrobenzoic acid) (DTNB) was used as the chromophoric reagent.²⁷ Inhibition assays were carried out on an Agilent 8453E UV–visible spectrophotometer equipped with a cell changer. Solutions of tested compounds were prepared starting from 10 mM stock solutions in DMSO, which were diluted with aqueous assay medium to a final content of organic solvent always lower than 1%. AChE inhibitory activity was determined in a reaction mixture containing 200 μ L of a solution of AChE (0.415 U/mL in 0.1 M phosphate buffer, pH 8.0), 100 μ L of a 3.3 mM solution of DTNB in 0.1 M phosphate buffer (pH 7.0) containing 6 mM NaHCO₃, 100 μ L of a solution of the inhibitor (six to seven concentrations ranging from 1×10^{-10} to 1×10^{-4} M), and 500 μ L of phosphate buffer, pH 8.0. After incubation for 20 min at 25 °C, acetylthiocholine iodide (100 μ L of 5 mM aqueous solution) was added as the substrate, and AChE-catalyzed hydrolysis was followed by measuring the increase of absorbance at 412 nm for 5.0 min at 25 °C. The concentration of compound which determined 50% inhibition of the AChE activity (IC₅₀) was calculated by nonlinear regression of the response–log(concentration) curve, using GraphPad Prism, version 5. BChE inhibitory activity was assessed similarly using butyrylthiocholine iodide as the substrate.

Kinetic studies on bovine AChE reported in Figure 5 were performed in the same incubation conditions, using six concentrations of substrate (from 0.033 to 0.2 mM) and four concentrations of compound **56** (from

0 to 30 nM). Apparent inhibition constants and kinetic parameters were calculated within the "enzyme kinetics" module of Prism.

Inhibition tests on human recombinant AChE (2770 U/mg) and human serum BChE (7.5 U/mg) were run under the same experimental conditions used for bovine AChE and horse BChE, respectively.

Choline Kinase Inhibition. The ex vivo ChoK inhibition assays for compound **56** were performed according to a previously reported protocol.⁴¹

Inhibition of A β _{1–40} Aggregation. A β _{1–40} (purity of >95%; EzBiolab, Carmel, CA, U.S.) was treated as previously reported²⁸ in order to obtain batches free from preaggregates. Inhibitory activities were determined for test compounds at 100 μ M in 30 μ M A β aggregation samples, using a previously described spectrofluorimetric method.²⁸

■ ASSOCIATED CONTENT

S Supporting Information. Docking models of **56** into BChE, ChoK, and TcAChE (Figures S1–S3). This material is available free of charge via the Internet at <http://pubs.acs.org>.

■ AUTHOR INFORMATION

Corresponding Author

*Phone: ++390805442782. Fax: ++39-0805442230. E-mail: carotti@farmchim.uniba.it

Author Contributions

[†]A.C.G. and L.P. contributed equally to this work.

■ ACKNOWLEDGMENT

The Spanish authors thank the Consejería de Innovación, Ciencia y Empresa of the Junta de Andalucía (Excellence Research Project No. P07-CTS-03210) for financial support and M. Paz Carrasco-Jiménez and Pablo Rios from the Department of Biochemistry and Molecular Biology, University of Granada (Spain), for the determination of ChoK IC₅₀ for compound **56**. Financial support to the Italian authors from MIUR (Rome, Italy; Grant PRIN 20085HR5JK) is gratefully acknowledged.

■ ABBREVIATIONS USED

A β , β -amyloid; ACh, acetylcholine; AChE, acetylcholinesterase; AD, Alzheimer's disease; BChE, butyrylcholinesterase; ChE, cholinesterase; ChoK, choline kinase; CNS, central nervous system; DTNB, 5,5'-dithiobis(2-nitrobenzoic acid); HB, hydrogen bond; MG, myasthenia gravis; NMB, neuromuscular blockade; PNS, peripheral nervous system; QAS, quaternary ammonium salt; SAFIR, structure–affinity relationship; SI, selectivity index; SSR, structure–selectivity relationship; THIQ, 1,2,3,4-tetrahydroisoquinolin-2-yl

■ REFERENCES

(1) Gentry, M. K.; Doctor, B. P. Alignment of Amino Acid Sequences of Acetylcholinesterases and Butyrylcholinesterases. In *Cholinesterases: Structure, Function, Mechanism, Genetics and Cell Biology*; Massoulié, J., Bacou, F., Barnard, E. A., Chatonnet, A., Doctor, B. P., Quinn, D. M., Eds.; American Chemical Society: Washington, DC, 1991; pp 394–398.

(2) Saxena, A.; Redman, A. M.; Jiang, X.; Lockridge, B. P.; Doctor, B. P. Differences in Active Site Gorge Dimensions of Cholinesterases Revealed by Binding of Inhibitors to Human Butyrylcholinesterase. *Biochemistry* **1997**, *36*, 14642–14651.

(3) Sussman, J. L.; Harel, M.; Frolow, F.; Oefner, C.; Goldman, A.; Toker, L.; Silman, I. Atomic Structure of Acetylcholinesterase from *Torpedo californica*: A Prototypic Acetylcholine-Binding Protein. *Science* **1991**, *253*, 872–879.

(4) Inestrosa, N. C.; Alvarez, A.; Perez, C. A.; Moreno, R. D.; Vicente, M.; Linker, C.; Casanueva, O. I.; Soto, C.; Garrido, J. Acetylcholinesterase Accelerates Assembly of Amyloid-beta-peptides into Alzheimer's Fibrils: Possible Role of the Peripheral Site of the Enzyme. *Neuron* **1996**, *16*, 881–891.

(5) Kryger, G.; Silman, I.; Sussman, J. L. Structure of Acetylcholinesterase Complexed with E2020 (Aricept): Implications for the Design of New Anti-Alzheimer Drugs. *Structure* **1999**, *7*, 297–307.

(6) Rama Sastry, B. V. Anticholinergic Drugs. In *Burger's Medicinal Chemistry and Drug Discovery*, 6th ed.; Abraham, D. J., Ed.; Wiley: New York, 2003; pp 109–166.

(7) Bevan, D. R.; Donati, F.; Kopman, A. F. Reversal of Neuromuscular Blockade. *Anesthesiology* **1992**, *77*, 785–805.

(8) Meriggioli, M. N.; Sanders, D. B. Autoimmune Myasthenia Gravis: Emerging Clinical and Biological Heterogeneity. *Lancet* **2009**, *8*, 475–490.

(9) McKinnon, S. J.; Goldberg, L. D.; Peeples, P.; Walt, J. G.; Bramley, T. J. Current Management of Glaucoma and the Need for Complete Therapy. *Am. J. Manag. Care* **2008**, *14*, S20–S27.

(10) García-Carrasco, M.; Escárcega, R. O.; Fuentes-Alexandro, S.; Riebeling, C.; Cervera, R. Therapeutic Options in Autoimmune Myasthenia Gravis. *Autoimmun. Rev.* **2007**, *6*, 373–378.

(11) (a) Pisani, L.; Catto, M.; Giangreco, I.; Leonetti, F.; Nicolotti, O.; Stefanachi, A.; Cellamare, S.; Carotti, A. Design, Synthesis and Biological Evaluation of Coumarin Derivatives Tethered to an Edrophonium-like Fragment as Highly Potent and Selective Dual Binding Site Acetylcholinesterase Inhibitors. *ChemMedChem* **2010**, *5*, 1616–1630. (b) Leonetti, F.; Catto, M.; Nicolotti, O.; Pisani, L.; Cappa, A.; Stefanachi, A.; Carotti, A. Homo- and Hetero-Bivalent Edrophonium-like Ammonium Salts as Highly Potent, Dual Binding Site AChE Inhibitors. *Bioorg. Med. Chem.* **2008**, *16*, 7450–7456.

(12) (a) Campos, J.; Núñez, M. C.; Conejo-García, A.; Sánchez-Martín, R. M.; Hernández-Alcoceba, R.; Rodríguez-González, A.; Lacal, J. C.; Gallo, M. A.; Espinosa, A. QSAR-Derived Choline Kinase Inhibitors: How Rational Can Antiproliferative Drug Design Be? *Curr. Med. Chem.* **2003**, *10*, 1095–1112. (b) Campos, J. M.; Sánchez-Martín, R. M.; Conejo-García, A.; Entrena, A.; Gallo, M. A.; Espinosa, A. (Q)SAR Studies To Design New Human Choline Kinase Inhibitors as Antiproliferative Drugs. *Curr. Med. Chem.* **2006**, *13*, 1231–1248.

(13) Campos, J.; Núñez, M. C.; Rodríguez, V.; Entrena, A.; Hernández-Alcoceba, R.; Fernández, F.; Lacal, J. C.; Gallo, M. A.; Espinosa, A. LUMO Energy of Model Compounds of Bispyridinium Compounds as an Index for the Inhibition of Choline Kinase. *Eur. J. Med. Chem.* **2001**, *36*, 215–225.

(14) Conejo-García, A.; Báñez-Coronel, M.; Sánchez-Martín, R.; Rodríguez-González, A.; Ramos, A.; Ramírez de Molina, A.; Espinosa, A.; Gallo, M. A.; Campos, J.; Lacal, J. C. Influence of the Linker in Bispyridinium Compounds on the Inhibition of Human Choline Kinase. *J. Med. Chem.* **2004**, *47*, 5433–5440.

(15) Sánchez-Martín, R.; Campos, J. M.; Conejo-García, A.; Cruz-López, O.; Báñez-Coronel, M.; Rodríguez-González, A.; Gallo, M. A.; Lacal, J. C.; Espinosa, A. Symmetrical Bis-Quinolinium Compounds: New Human Choline Kinase Inhibitors with Antiproliferative Activity against the HT-29 Cell Line. *J. Med. Chem.* **2005**, *48*, 3354–3363.

(16) Campos, J.; Núñez, M. C.; Sánchez, R. M.; Gómez-Vidal, J. A.; Rodríguez-González, A.; Báñez, M.; Gallo, M. A.; Lacal, J. C.; Espinosa, A. Quantitative Structure–Activity Relationships for a Series of Symmetrical Bisquaternary Anticancer Compounds. *Bioorg. Med. Chem.* **2002**, *10*, 2215–2231.

(17) Rosa, J. C.; Galanakis, D.; Ganellin, C. R.; Dunn, P. M. Synthesis, Molecular Modeling, and K⁺ Channel-Blocking Activity of Dequalinium Analogues Having Semirigid Linkers. *J. Med. Chem.* **1996**, *39*, 4247–4254.

- (18) Conejo-García, A.; Campos, J.; Sánchez-Martín, R. M.; Gallo, M. A.; Espinosa, A. Bispyridinium Cyclophanes: Novel Templates for Human Choline Kinase Inhibitors. *J. Med. Chem.* **2003**, *46*, 3754–3757.
- (19) Conejo-García, A.; Campos, J.; Sánchez, R. M.; Rodríguez-González, A.; Lacal, J. C.; Gallo, M. A.; Espinosa, A. Choline Kinase Inhibitory Effect and Antiproliferative Activity of New 1,1',1''-(Benzene-1,3,5-triylmethylene)tris{4-[(disubstituted)amino]pyridinium} Tribromides. *Eur. J. Med. Chem.* **2003**, *38*, 109–116.
- (20) Conejo-García, A.; Campos, J.; Sánchez, R. M.; Rodríguez-González, A.; Lacal, J. C.; Gallo, M. A.; Espinosa, A. Synthesis and NMR Studies on a C3-Symmetrical Triquinoline Triscationic Bicyclopentane. *J. Org. Chem.* **2005**, *70*, 5748–5751.
- (21) Tao, B.; Huang, T. L.; Zhang, Q.; Jackson, L.; Queener, S. F.; Donkor, I. O. Synthesis and Anti-*Pneumocystis carinii* Activity of Conformationally Restricted Analogues of Pentamidine. *Eur. J. Med. Chem.* **1999**, *34*, 531–538.
- (22) Neset, S.; Hope, H.; Undheim, K. Stereoselective Synthesis of Cyclopropane-1,2-bis(glycine) Derivatives. *Tetrahedron* **1997**, *53*, 10459–10470.
- (23) Wenner, W. Bis(bromomethyl) Compounds. *J. Org. Chem.* **1952**, *17*, 523–528.
- (24) Cram, D. J.; Steinberg, H. Macro Rings. I. Preparation and Spectra of the Paracyclophanes. *J. Am. Chem. Soc.* **1951**, *73*, 5691–5704.
- (25) Raston, I.; Wennerström, O. [2(6)]Paracyclophanes—Large Ring Compounds with Extended pi-Systems. *Acta Chem. Scand.* **1982**, *B36*, 655–660.
- (26) Drefahl, G.; Ploetner, G. Untersuchungen über Stilbene, XVIII. Polyphenyl-polyene. *Chem. Ber.* **1958**, *91*, 1274–1280.
- (27) Ellman, G. L.; Courtney, K. D.; Andres, V., Jr.; Feartherstone, R. M. A New and Rapid Colorimetric Determination of Acetylcholinesterase Activity. *Biochem. Pharmacol.* **1961**, *7*, 88–95.
- (28) Cellamare, S.; Stefanachi, A.; Stolfi, D. A.; Basile, T.; Catto, M.; Campagna, F.; Sotelo, E.; Acquafredda, P.; Carotti, A. Design, Synthesis, and Biological Evaluation of Glycine-Based Molecular Tongs as Inhibitors of A β ₁₋₄₀ Aggregation in Vitro. *Bioorg. Med. Chem.* **2008**, *16*, 4810–4822.
- (29) Verdonk, M. L.; Cole, J. C.; Hartshorn, M. J.; Murray, C. W.; Taylor, R. D. Improved Protein–Ligand Docking Using GOLD. *Proteins* **2003**, *52*, 609–623.
- (30) Hong, B. S.; Allali-Hassani, A.; Tempel, W.; Finerty, P. J., Jr.; MacKenzie, F.; Dimov, S.; Vedadi, M.; Park, H. Crystal Structures of Human Choline Kinase Isoforms in Complex with Hemicholinium-3: Single Amino Acid near the Active Site Influences Inhibitor Sensitivity. *J. Biol. Chem.* **2010**, *285*, 16330–16340.
- (31) Case, D. A.; Darden, T. A.; Cheatham, T. E., III; Simmerling, C. L.; Wang, J.; Duke, R. E.; Luo, R.; Crowley, M.; Walker, R. C.; Zhang, W.; Merz, K. M.; Wang, B.; Hayik, S.; Roitberg, A.; Seabra, G.; Kolossváry, I.; Wong, K. F.; Paesani, F.; Vanicek, J.; Wu, X.; Brozell, S. R.; Steinbrecher, T.; Gohlke, H.; Yang, L.; Tan, C.; Mongan, J.; Hornak, V.; Cui, G.; Mathews, D. H.; Seetin, M. G.; Sagui, C.; Babin, V.; Kollman, P. A. AMBER, version 10; University of California: San Francisco, CA, 2008.
- (32) Phillips, J. C.; Braun, R.; Wang, W.; Gumbart, J.; Tajkhorshid, E.; Villa, E.; Chipot, C.; Skeel, R. D.; Kale, L.; Schulten, K. Scalable Molecular Dynamics with NAMD. *J. Comput. Chem.* **2005**, *26*, 1781–1802.
- (33) Barril, X.; Orzoco, M.; Luque, F. J. Predicting Relative Binding Free Energies of Tacrine–Huperzine A Hybrids as Inhibitors of Acetylcholinesterase. *J. Med. Chem.* **1999**, *42*, 5110–5119.
- (34) Piazzini, L.; Rampa, A.; Bisi, A.; Gobbi, S.; Belluti, F.; Cavalli, A.; Bartolini, M.; Andrisano, V.; Valenti, P.; Recanatini, M. 3-(4-[(Benzyl(methyl)amino)methyl]-phenyl)-6,7-dimethoxy-2H-2-chromenone (AP2238) Inhibits Both Acetylcholinesterase and Acetylcholinesterase-Induced β -Amyloid Aggregation: A Dual Function Lead for Alzheimer's Disease Therapy. *J. Med. Chem.* **2003**, *46*, 2279–2282.
- (35) Campiani, G.; Fattorusso, C.; Butini, S.; Gaeta, A.; Agnusdei, M.; Gemma, S.; Persico, M.; Catalanotti, B.; Savini, L.; Nacci, V.; Novellino, E.; Holloway, H. W.; Greig, N. H.; Belinskaya, T.; Fedorko, J. M.; Saxena, A. Development of Molecular Probes for the Identification of Extra Interaction Sites in the Mid-Gorge and Peripheral Sites of Butyrylcholinesterase (BuChE). Rational Design of Novel, Selective, and Highly Potent BuChE Inhibitors. *J. Med. Chem.* **2005**, *48*, 1919–1929.
- (36) Cheng, Y.; Cheng, X.; Radić, Z.; McCammon, J. A. Acetylcholinesterase: Mechanisms of Covalent Inhibition of Wild-Type and H447I Mutant Determined by Computational Analysis. *J. Am. Chem. Soc.* **2007**, *129*, 6562–6570.
- (37) Jones, G.; Willett, P.; Glen, R. C.; Leach, A. R.; Taylor, R. Further Development of a Genetic Algorithm for Ligand Docking and Its Application to Screening Combinatorial Libraries. In *Rational Drug Design, Novel Methodology and Practical Applications*; Parrill, A. L., Reddy, M. R., Eds.; American Chemical Society: Washington, DC, 1999; pp 271–291.
- (38) Camps, P.; Formosa, X.; Galdeano, C.; Gómez, T.; Muñoz-Torrero, D.; Ramírez, L.; Viayna, E.; Gómez, E.; Isambert, N.; Lavilla, R.; Badia, A.; Clos, M. V.; Bartolini, M.; Mancini, F.; Andrisano, V.; Bidon-Chanal, A.; Huertas, Ó.; Dafni, T.; Luque, F. J. Tacrine-Based Dual Binding Site Acetylcholinesterase Inhibitors as Potential Disease-Modifying Anti-Alzheimer Drug Candidates. *Chem.-Biol. Interact.* **2010**, *187*, 411–415.
- (39) Muñoz-Ruiz, P.; Rubio, L.; Garcia-Palomero, E.; Dorronsoro, I.; del Monte-Millan, M.; Valenzuela, R.; Usan, P.; de Austria, C.; Bartolini, M.; Andrisano, V.; Bidon-Chanal, A.; Orozco, M.; Luque, F. J.; Medina, M.; Martínez, A. Design, Synthesis, and Biological Evaluation of Dual Binding Site Acetylcholinesterase Inhibitors: New Disease-Modifying Agents for Alzheimer's Disease. *J. Med. Chem.* **2005**, *48*, 7223–7233.
- (40) Hartshorn, M. J.; Verdonk, M. L.; Chessari, G.; Brewerton, S. C.; Mooij, W. T. M.; Mortenson, P. N.; Murray, C. W. Diverse, High-Quality Test Set for the Validation of Protein–Ligand Docking Performance. *J. Med. Chem.* **2007**, *50*, 726–741.
- (41) (a) Hernandez-Alcoceba, R.; Fernandez, F.; Lacal, J. C. In Vivo Antitumor Activity of Choline Kinase Inhibitors: A Novel Target for Anticancer Drug Discovery. *Cancer Res.* **1999**, *59*, 3112–3118. (b) Ramirez de Molina, A.; Penalva, V.; Lucas, L.; Lacal, J. C. Regulation of Choline Kinase Activity by Ras Proteins Involves Ral-GDS and PI3K. *Oncogene* **2002**, *21*, 937–994.